AD-A160 535 THE EFFECT OF SURFACE CONDITIONS ON THE MACH REFLECTION PHENOMENON(U) BEN-GURION UNIV OF THE NEGEV BEERSHEBA (ISRAEL) G BEN-DOR SEP 85 DAJA45-83-C-0046 1/1

UNCLASSIFIED F/G 20/4 NL

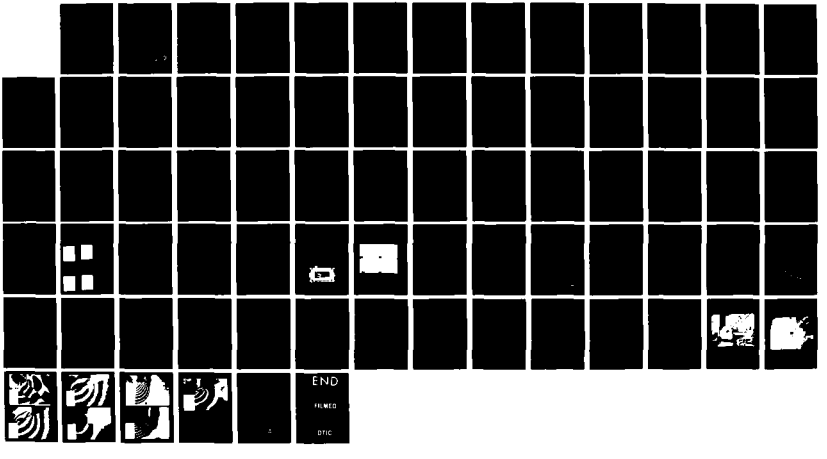

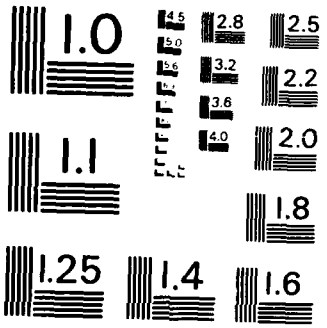

(4)

The Effect of Surface Conditions on the Mach Reflection Phenomenon

Dr. G. Ben-Dor

Ben-Gurion University of the Negev

Contract Number: DAJA 45-83-C-0046

Final Report

1 March 85 - 31 August 85

The research reported in this document has been made possible through the support and sponsorship of the U.S. Government through its European Research Office of the U.S. Army.

SECURITY CLASSIFICATION OF THIS PAGE (When Data Entered)

R&D 4200-PH

REPORT DOCUMENTATION PAGE

READ INSTRUCTIONS BEFORE COMPLETING FORM

1. REPORT NUMBER	2. GOVT ACCESSION NO.	3. RECIPIENT'S CATALOG NUMBER
	AD-A160 535	

4. TITLE (and Subtitle)

The Effect of Surface Conditions on the Mach Reflection Phenomenon

5. TYPE OF REPORT & PERIOD COVERED

Final Report
~~Jul 83 — Sep 85~~ 1MAR-31AUG.85

6. PERFORMING ORG. REPORT NUMBER

7. AUTHOR(s)

Dr. G. Ben-Dor

8. CONTRACT OR GRANT NUMBER(s)

DAJA45-83-C-0046

9. PERFORMING ORGANIZATION NAME AND ADDRESS

Ben-Gurion University of the Negev
Beer Sheva, Israel

10. PROGRAM ELEMENT, PROJECT, TASK AREA & WORK UNIT NUMBERS

61102A
1L161102BH57-07

11. CONTROLLING OFFICE NAME AND ADDRESS

USARDSG-UK
Box 65, FPO NY 09510-1500

12. REPORT DATE

September 1985

13. NUMBER OF PAGES

72

14. MONITORING AGENCY NAME & ADDRESS (if different from Controlling Office)

15. SECURITY CLASS (of this report)

Unclassified

15a. DECLASSIFICATION/DOWNGRADING SCHEDULE

16. DISTRIBUTION STATEMENT (of this Report)

Approved for Public Release; distribution unlimited

17. DISTRIBUTION STATEMENT (of the abstract entered in Block 20, if different from Report)

18. SUPPLEMENTARY NOTES

19. KEY WORDS (Continue on reverse side if necessary and identify by block number)

Shock wave; Regular and Mach reflections; Boundary layer; Reflecting wedge; Pseudo-steady flow; Surface roughness; Von Neuman paradox.

20. ABSTRACT (Continue on reverse side if necessary and identify by block number)

The aim of the present study was to study both experimentally and analytically the effect of the surface conditions on the shock reflection phenomenon. In general, the study was divided into two parts:

1) the reflection of a planar shock wave over rough surfaces, and
2) the reflection of a planar shock wave over a liquid surface.

In accordance with these two parts, the following final report is also divided into two parts.

DD FORM 1 JAN 73 1473 EDITION OF 1 NOV 65 IS OBSOLETE

UNCLASSIFIED

SECURITY CLASSIFICATION OF THIS PAGE (When Data Entered)

Introduction

The aim of the present study was to study both experimentally and analytically the effect of the surface conditions on the shock reflection phenomenon.

In general, the study was divided into two parts:

1) the reflection of a planar shock wave over rough surfaces, and

2) the reflection of a planar shock wave over a liquid surface.

In accordance with these two parts, the following final report is also divided into two parts.

PART 1

The reflection of a planar shock wave over rough surfaces.

Abstract

The effect of surface roughness on the transition from regular (RR) to Mach reflection (MR) over straight wedges in pseudo-steady flows was investigated both experimentally and analytically.

Two models for predicting the RR $\neq$ MR transition in the (M_s, θ_w)-plane were developed (M_s is the incident shock wave Mach number and θ_w is the reflecting wedge angle). Their validity was checked against experimental results. Since the experimental results are limited to the ranges $1 < M_s \leq 2$ and $3.5 < M \leq 4$ and surface roughness heights of $0 < \varepsilon \leq 0.2$ cm, the proposed models are applicable to these ranges only. In the first model (the pressure loss model), the transition from RR to MR is assumed to be related to the pressure loss due to the increased friction between the flow and the rough surface. In the second model (the boundary layer displacement thickness model), the RR $\neq$ MR transition is related to the boundary layer displacement thickness which in turn depends on the surface roughness.

It was shown that the boundary layer displacement thickness δ^* could be characterized by the parameter $G = \frac{\delta_L V_*}{\nu}$ (where δ_L is the laminar sublayer thickness, V_* is the shear velocity and ν is the kinematic viscosity). This parameter was found to be constant for a given size of surface roughness - ε i.e., G was found to be independent of the incident shock wave Mach number - M_s . Owing to this fact G was termed the "roughness characterizer."

Introduction

When a planar incident normal shock wave encounters a sharp corner in a shock tube, four different types of reflection can occur depending on the incident shock wave Mach number -M_s and the wedge angle - θ_w. They are:

1) regular reflection - RR (figure 1a),

2) single-Mach reflection - SMR (figure 1b),

3) complex-Mach reflection - CMR (figure 1c), and

4) double-Mach reflection - DMR (figure 1d).

The latter three types, i.e., SMR, CMR and DMR are usually termed as Mach reflections - MR .

The RR $\rightleftarrows$ MR transition criterion in pseudo-steady flows (the "detachment criterion") was first introduced by von Neumann (1963). In developing this criterion von Neumann assumed that:

1) the flow is ideal, i.e.,. $\mu = 0$ and $k = 0$ (μ is the dynamic viscosity and k is the heat conductivity),

2) the flow is two-dimensional, and

3) the flow is self-similar and hence pseudo-steady.

As shown by Ben-Dor & Glass (1979), the detachment criterion can be expressed as follows:

$$\theta_1 + \theta_{2m} = 0 \qquad (1)$$

where θ_1 is the flow deflection through the incident shock wave - i, and θ_{2m} is the maximum possible flow deflection through the reflected shock wave - r. This formulation is based on the fact that when the frame of reference is attached to the reflection point - G (see figure 2) the flow ahead of the incident shock wave - i, which now moves parallel to the wedge surface at supersonic velocity $v_o = u_s/\cos\theta_w$ (u_s is the incident shock wave velocity), is deflected towards the wedge by an angle θ_1 . Thus the supersonic flow behind the incident shock wave - i is deflected

towards the solid surface. In order to negotiate the solid surface it must experience a reflection while crossing the reflected shock wave r to become again parallel to the wedge surface. When the angle θ_2 exceeds the maximum deflection angle θ_{2m}, the regular reflection becomes theoretically impossible. Consequently equation (1) represents the "detachment" criterion of von Neumann.

However, the experimental findings of von Neumann (1943), Smith (1945), Taub (1947), Bleakney & Taub (1949), Fletcher (1950), White (1951), Law & Glass (1971), Henderson & Lozzi (1975), Ben-Dor (1978), Henderson & Woolington (1983) and Hornung & Taylor (1982) indicates that the RR exists beyond the predicted theoretical limit of the "detachment" criterion.

The transition line predicted by the "detachment" criterion (equation 1), as well as our experimentally obtained RR $\rightleftarrows$ MR transition points are shown in figure 3. The persistance of the RR beyond the limit predicted by the detachment criterion is clearly seen. Since the von Neumann paradox was first noticed, many scientists [Henderson & Lozzi (1975), Ben-Dor & Glass (1979), Henderson & Woolmington (1983), Hornung & Taylor (1982)] directed their efforts at resolving this paradox. Probably the most promising approach was the one suggested by Hornung & Taylor (1982). They argued that the reason for the existence of the von Neumann paradox is the fact that the transition line was derived by solving the inviscid flow conservation equations while the actual flow was viscous. Consequently, they concluded that by accounting for viscous effects the von Neumann paradox could be resolved. Hornung & Taylor (1982) accounted for the viscous effects by applying the boundary layer displacement thickness concept. The obtained results justified their approach.

Takayama, Gotoh and Ben-Dor (1981) presented experimental results regarding RR $\rightleftarrows$ MR transition over rough surfaces. Their results are reproduced in figure 4. The difference between the actual transition and the values predicted by the detachment criterion (solid line) is quite clear. This difference increases as the roughness

neight increases. For example, at M_s = 4 and ε = 0.2 cm, the actual wedge angle at which the RR ⇄ MR transition occurs is about 20° lower than that predicted by the "detachment" criterion.

The fact that the surface roughness has such a meaningful influence on the transition wedge angle on one hand, and the fact that shock reflections, in nature, occur over rough surfaces, has led to the recognition that understanding the reflection process over rough surfaces is of great importance. Consequently, models capable of predicting the RR ⇄ MR transition over rough surfaces were sought. This was further stressed in the first concluding remark of the 3rd Mach Reflection Symposium (held in Melbourne, Austrlia, in August 1983) which said: "It appears to be the boundary layer which causes the delay of the transition from regular to Mach reflection of pseudo-stationary shocks beyond the detachment or maximum deflection point for reflection from a plane surface. This effect is more pronounced in the case of rough surfaces."

Based on the foregoing discussion the RR ⇄ MR transition process was investigated both experimentally and analytically. Since Hornung & Taylor (1982) were able to explain the von Neumann paradox by including the viscous effect in their solution of the flow field, it was decided to base the present models for predicting the RR ⇄ MR transition over rough surfaces on "viscous mechanisms."

Subsequently, two different approaches through which the effect of viscosity can be accounted for will be proposed. In the first, the pressure loss due to friction is integrated into the inviscid conservation equations, while in the second the wedge geometry is modified using the boundary layer displacement thickness concept.

Experimental Results

The experimental results reported here were obtained using the 40 x 80 mm shock tube of the IHSM Institute of High Speed Mechanics, Tohoku University, Sendai, Japan. An illustration of the "saw-tooth" roughness imposed on the tested wedge models is

given in figure 5a. For the first set of experiments four models (each 4 cm long) with roughness of ε = 0.01, 0.02, 0.08 and 0.2 cm were prepared. The effective wedge angle of the models could be adjusted from outside the shock tube test section as shown in figure 5b. The experimental study covered the range of $1 < M_s \leq 4$.

The shock wave velocity was measured using Kistler 606 pressure tranducers, an Iwatsu UC 7641 digital counter and an Iwatsu DM 901 recorder. The pressure tranducers were mounted 120 mm apart just ahead of the test section. The attenuation of the incident shock wave was found to be negligibly small.

The test gas was pure nitrogen. The initial pressures were in the range of $3 \leq P_o \leq 150$ torr. For the investigated range of Mach numbers ($1 < M_s \leq 4$) the nitrogen gas can be assumed to behave as a perfect gas. Therefore, the initial pressure has no effect on the reflection phenomenon. For all the experiments the initial temperature was about T_o = 300K.

An optical diagnostic (shadowgraph) was used for studying the pseudo-steady reflection phenomenon. A pulsed ruby laser (6943 A) was used as a light source. Typical shadowgraphs are shown in figures 6a to 6d. Mach reflection over a wedge having roughness height of ε = 0.02 cm is shown in figure 6a. Regular reflection over the same wedge is shown in figure 6b. Figures 6c and 6d show a MR and a RR over a wedge having roughness height of ε = 0.2 cm, respectively.

The RR ⇌ MR transition angle was determined in the following way. For a given value of the incident shock wave Mach number - M_s the wedge angle θ_w was gradually increased until a RR was obtained. Then, the value of the triple point trajectory angle χ (deduced from the shadowgraphs) was plotted in the (χ, θ_w)-plane as shown in figure 7. The experimental results were then extrapolated to $\chi = 0$. The wedge angle at this point was chosen as the transition wedge angle - $\theta_{w,tr}$. This procedure yields $\theta_{w,tr}$ to an accuracy of $\pm 1°$. The above-mentioned procedure was repeated for M_s = 1.04, 1.12, 1.21, 1.44, 1.96, 3.58, 3.77 and 3.89.

The experimental results obtained for the four different models, as well as the

results obtained for a "smooth" model, are shown in figure 4.

It is apparent that the surface roughness (ε) has a significant influence on the RR $\rightleftarrows$ MR transition wedge angle for any given incident shock wave Mach number. The greater ε is, the smaller is the transition wedge angle $\theta_{w,tr}$. It is of interest to note that the measured transition wedge angles over the smooth surface model does not agree with the "detachment" criterion (these results confirm the von Neumann paradox). Had the surface been perfecty smooth, i.e., $\varepsilon = 0$, the experimental results should have agreed with the "detachment" criterion. However, since no surface is perfectly smooth, the von Neumann paradox exists. In the following we will refer to a "smooth" surface as hydraulically-smooth. Furthermore, it will be proven analytically that a hydraulically smooth surface is a surface for which $\varepsilon \leq 0.00517$ cm.

Analysis

As mentioned previously the aim of the present study is to develop models capable of predicting the RR $\rightleftarrows$ MR transition over rough surfaces, i.e., models which will shift the "detachment" transition line (solid line in figure 4) towards the experimental results for any given roughness height of $\sim \varepsilon$.

General Assumptions

1) The flow is two-dimensional.

2) The flow field can be described by the mass, momentum and energy conserrvation equations of inviscid flows with additional terms accounting for viscous effects.

3) The flow is self-similar, and hence, can be made pseudo-steady by applying the well-known Galilian transformation.

4) Real gas effects can be ignored, consequently the gas is assumed to obey the equation of state of a perfect gas. (i.e., $P = \rho RT$).

The Conservation Equations

The wave configuration of a RR is shown schematically in figure 2. Employing the foregoing assumptions, and attaching the frame of reference to the reflection point G (in such a way that it moves along the wedge surface together with point G) results in the following nine equations which completely describe the flow field in the vicinity of the reflection point - G.

across the incident shock wave i:

continuity

$$\rho_o v_o \sin\phi_o = \rho_1 v_1 \sin(\phi_o - \theta_1) \tag{2}$$

tangentional momentum

$$\rho_o \tan\phi_o = \rho_1 \tan(\phi_o - \theta_1) \tag{3}$$

normal momentum

$$P_o + \rho_o v_o^2 \sin^2\phi_o = P_1(1-F_p) + \rho_1 v_1^2 \sin^2(\phi_o - \theta_1) \tag{4}$$

energy

$$h_o + \frac{1}{2} v_o^2 \sin^2\phi_o = h_1 + \frac{1}{2} v_1^2 \sin^2(\phi_o - \theta_1) \tag{5}$$

across the reflected shock wave r:

continuity

$$\rho_1 v_1 \sin\phi_1 = \rho_2 v_2 \sin(\phi_1 - \theta_2) \tag{6}$$

tangentional momentum

$$\rho_1 \tan\phi_1 = \rho_2 \tan(\phi_1 - \theta_2) \tag{7}$$

normal momentum

$$P_1(1-F_P) + \rho_1 v_1^2 \sin^2\phi_1 = P_2(1-F_P) + \rho_2 v_2^2 \sin^2(\phi_1-\theta_2) \quad (8)$$

energy

$$h_1 + \frac{1}{2} v_1^2 \sin^2\phi_1 = h_2 + \frac{1}{2} v_2^2 \sin^2(\phi_1-\theta_2) \quad (9)$$

and the boundary condition for the RR $\rightleftarrows$ MR transition:

$$\theta_1 + \theta_{2m} = \alpha \quad (10)$$

Setting $F_P = 0$ and $\alpha = 0$ results in the well-known set of equations describing a regular reflection in an inviscid flow. The solution of these equations, which yields the "detachment" transition line (shown in figures 3 and 4), can be found in Ben-Dor's (1978) work. Note that $v_o = u_s/\cos\theta_w$, $\phi_o = 90-\theta_w$, P_o and T_o are known. The enthalpy h is related to the tempertaure through $h = C_P T$ and the density ρ can be calculated from the equation of state for a perfect gas, i.e., $\rho = P/RT$. The definitions of ϕ_o, ϕ_1, θ_1 and θ_2 are shown in figure 2.

The Roughness Effect on the Turbulent Flow

Usually, surfaces over which fluids flow cannot be considered as perfectly smooth. Experiments have indicated that the roughness height - ε significantly contributes to the friction coefficient - f. Owing to this fact it is necessary to develop models which will relate the friction coefficient f to the roughness height - ε. This is done in the following.

Blasius [Schlichting (1962)] showed experimentally that for hydraulically smooth pipes the friction coefficient f depends solely on the Reynolds number (Re). Nopf (1923) found experimentally that for very rough pipes the friction coefficient f depends solely on the relative roughness ε/R (R is the pipe radius). Furthermore, he showed that for less rough pipes f depends both on Re and ε/R. These experimental

findings suggested that the considered phenomenon is controlled by the thickness of the laminar sublayer - δ_L . Their conclusion was that the dominant factor in determining the value of the friction coefficient f is ε/δ_L. When $\varepsilon < \delta_L$ (i.e., the surface roughness is completely immersed inside the laminar sublayer) the roughness has practically no effect on f, and the surface can be considered as "hydraulically smooth." On the other hand, for $\varepsilon >> \delta_L$ the roughness has a dominant effect on f. In such a case the friction mechanism is known as "wave drag" [Shames (1962)]. It was further shown by Schlichting (1962) that for any given size of roughness, $\frac{v_* \delta_L}{\nu}$ = const (v_* is the shear velocity and ν is the kinematic viscosity). This finding led Schlichting to derive the following relation:

$$\frac{\varepsilon}{\delta_L} \sim \frac{\varepsilon v_*}{\nu} \qquad (11)$$

It is clear from this relation that $\frac{\varepsilon v_*}{\nu}$ can replace $\frac{\varepsilon}{\delta_L}$ and therefore be considered as the dominant factor in determining the value of the friction coefficient.

Based on the experimental results of Nikuradsse (1933) it is a common practice to divide the turbulent flow over rough surfaces into three flow zones [Shames (1962)].

1) hydraulically smooth flow: $\frac{\varepsilon}{\delta_L} < 1$ or $\frac{\varepsilon v_*}{\nu} < 5$ and $f = f(Re)$

2) frictional transition flow: $1 < \frac{\varepsilon}{\delta_L} < 15$ or $5 < \frac{\varepsilon v_*}{\nu} < 70$ and $f = f(Re, \varepsilon/R)$

3) rough flow: $\frac{\varepsilon}{\delta_L} > 15$ or $\frac{\varepsilon v_*}{\nu} > 70$ and $f = f(\varepsilon/R)$

Once the turbulent character of the flow is defined, it is important to have correlations relating the roughness to the friction losses. As a basis for constructing such correlations the following logarithmic velocity distribution law is used:

$$\frac{\bar{u}}{v_*} = \frac{1}{\alpha_1} [\ln \frac{v_* y}{\nu} - \ln\beta] \qquad (12)$$

where $\bar{u}$ is the time average velocity, α_1 is a universal constant, y is the distance coordinate measured from the surface and β is a constant depending on the roughness height - ε. The assumptions under which the logaritmic velocity distribution law was obtained are given by Prandtl (1925). Detailed derivation of equation (12) can be found in Shames (1962). A comparison between the experimental results of Nikuradse (1933) and equation (12) indicates that:

1) for a large range of Reynolds numbers and roughness heights, $\alpha_1 = 0.4$.

2) for a hydraulically smooth flow

$$\ln\beta = -2.2 \tag{13}$$

for the frictional transition flow,

$$-2.2 \leq \ln\beta \leq 0.8 \tag{14}$$

and for the rough flow

$$\ln\beta = \ln\frac{\varepsilon v_*}{\nu} - 3.4 \tag{15}$$

Based on these values of α_1 and β expressions for evaluating the friction coefficient - f, for flat plates, were derived for each of the three flow zones. In order not to limit the present results to any specific flow zone a different analytical approach is taken in the present study. This approach is outlined in the following.

Inserting the boundary condition $u\big|_{y=\delta_L} = u_L$ (figure 8) into equation (12) yields

$$\frac{u_L}{v_*} = \frac{1}{\alpha_1}\left[\ln\frac{v_*\delta_L}{\nu} - \ln\beta\right] \tag{16}$$

In the laminar sublayer the velocity changes linearily therefore

$$u_L = \frac{\tau_w}{\mu}\delta_L \tag{17}$$

where τ_w is the shear stress on the surface. Inserting the relation $v_*^2 = \tau_w/\rho$

$$\frac{u_L}{v_*} = \frac{v_* \delta_L}{\nu} \tag{18}$$

Combining equations (16) and (18) yields:

$$G = \frac{1}{\alpha_1} (\ln G - \ln \beta) \tag{19}$$

where $G \equiv \frac{v_* \delta_L}{\nu}$

For $\alpha_1 = 0.4$ equation (19) reduces to

$$G = 2.5(\ln G - \ln \beta) \tag{20}$$

Since β depends solely on the roughness height ϵ, it is obvious from equation (20) that so does G, i.e., for any given value of ϵ, the value of G is independent of the flow properties. It was therefore decided to call G the "roughness characterizer".

It should be noted that the roughness characterizer $G = \frac{v_* \delta_L}{\nu}$ is simply the common Reynolds number in the usual form applicable to the inner layer. The laminar sublayer thickness δ_L is fundamental in the evaluation of G. Indeed, G does characterize the roughness effects, but should more properly be viewed as the ratio of two length scales; δ_L and a viscous length $\frac{\nu}{v^*}$

For assessing the value of G appropriate to hydraulically smooth surfaces, Blasius' results can be used. Blasius found [Schlichting (1982)] that the friction coefficient for the considered case is given by:

$$f = 0.3164 \, R_{e,D}^{-1/4} \tag{21}$$

where $R_{e,D} = \frac{u_{av} D}{\nu}$. Equation (21), which is known as the Blasius equation, was derived for the following specific velocity profile:

$$\frac{\bar{u}}{u_o} = \left(\frac{y}{R}\right)^{\frac{1}{7}} \tag{22}$$

For a general velocity profile,

$$\frac{\bar{u}}{u_o} = \left(\frac{y}{R}\right)^{n} \tag{23}$$

equation (21) can be generalized to the following form:

$$f = C(n,G) \, Re^{-\frac{2n}{n+1}}$$

In this relation the velocity power exponent n depends solely on the Reynolds number (Shames, 1982). Mazor (1984) showed that C(n,G) has the following form,

$$G(n,G) = 2^{\frac{5n+1}{n+1}} [(n+1)(n+2)]^{\frac{2}{n+1}} G^{\frac{2(n+1)}{n+1}} \qquad (25)$$

Inserting $n = \frac{1}{7}$ into equation (25) and recalling that for this value of n, C(n,G) = 0.3164 [see equation (21)] yields for a hydraulically smooth surface

$$G = 12.2468$$

Using this value of G in equation (20) implies that for a hydraulically smooth surface

$$\ln\beta = -2.39$$

This value of $\ln\beta$ is about 8% smaller than the value usually quoted in the literature [equation (13)].

The value of the roughness characterizer - G for a frictional transition flow can be determined from equation (20). As mentioned earlier, for a frictional transition flow $-2.2 \leq \ln\beta \leq 0.8$ [equation (15)], thus by inserting $\ln\beta = 0.8$ into equation (20), the lower value of G for a frictional transition flow can be obtained.

Following this procedure one finally obtains:

- for the hydraulically smooth flow G = 12.2468
- for the frictional transition flow $0.5625 < G < 12.2468$
- for the rough flow $0 < G < 0.5625$

Models for Predicting the Effect of the Surface Roughness on the RR $\rightleftarrows$ MR Transition

As mentioned, the detachment criterion of von Neumann (1963) does not agree with experimental results. By accounting for viscous effects, Hornung & Taylor (1982) were able to explain the discrepancy.

For rough surfaces, where viscous effects are much more pronounced, the inviscid model [equations (2) to (10)] predict the RR $\rightleftarrows$ MR transition very poorly. In the

following, two models for predicting the RR $\rightleftarrows$ MR transition over rough surfaces are developed. The formulation of these models is similar to the inviscid flow model, with additional terms accounting for viscous effects.

The Pressure Loss-Model

Viscosity results in pressure losses. Therefore it is natural to express its effects on the flow field by introducing a pressure loss term in the inviscid conservation equations. Since ahead of the incident shock wave the flow is quiescent, only the pressures in states (1) and (2) [see figure 2] need to be corrected. Consequently, a pressure loss coefficient F_p, which depends on both the roughness height ϵ and the inverse pressure ratio across the incident shock wave - ξ is introduced into the conservation equations for inviscid flow. This pressure loss coefficient can be expressed as

$$\Delta P = F_p(\epsilon,\xi)\,(P_1-P_2) \qquad (26)$$

Thus equations (2) to (10) with $F_p \neq 0$ and $\alpha = 0$ represent the conservation equations for the pressure loss model.

Takayama, Gotoh & Ben-Dor (1981) showed that the pressure loss coefficient can be expressed as follows:

$$F_p(\epsilon,\xi) = F_\epsilon\,(1-\xi)^\eta \qquad (27)$$

where F_ϵ depends on the roughness height ϵ only and η is a constant; η can be found from the experimental results. Their experimental data indicated that $\eta = 7/9$. The RR $\rightleftarrows$ MR transition lines, as predicted by equations (2) to (10) for $F_p \neq 0$ and $\alpha = 0$ were fitted to the experimental results of Takayama, Goton and Ben-Dor (1981) by choosing appropriate values for F_ϵ. The obtained results are shown in figure 9. The values of F_ϵ which resulted in the desired shift of the RR $\rightleftarrows$ MR transition lines (to fit the experimental results) are listed in figure 9. It is apparent from figure 9 that the experimentally obtained transitions for hydraulically smooth surfaces can

best be described by $F_\varepsilon = 0.1$. The value $F_\varepsilon = 0$ corresponds exactly to the "detachment" transition criterion of von Neumann, [i.e., a perfectly smooth surface ($\varepsilon = 0$)].

In order to complete this model, the values of F_ε were correlated to the roughness height

$$F_\varepsilon = -545.45\ \varepsilon^2 + 31.73\varepsilon - 0.012; \text{ for } 0 \leq \varepsilon \leq 0.02 \text{ cm} \quad (28)$$

and

$$F_\varepsilon = -4.63\ \varepsilon^2 + 2.55\varepsilon + 0.35; \text{ for } 0.02 \leq \varepsilon \leq 0.2 \text{ cm} \quad (29)$$

These correlations along with the measured values of ($F_\varepsilon - \varepsilon$) are shown in figure 10.

In summary, the proposed model should be used as follows. For any given value surface roughness ε (in cm) one evaluates F_ε using equations (28) or (29). Then F_P is calculated by equation (27). Subsequently this value is used in the conservation equations [(2) to (10)]. It should be noted that for the pressure loss model α [equation (10)] should be kept equal to zero.

The Boundary Layer Displacement Thickness Model

The idea to account for the viscous effects through the boundary layer displacement thickness is due to Hornung & Taylor (1982) who resolved the von Neumann paradox by applying this concept.

The boundary layer displacement thickness - δ^* is defined as the distance by which the solid boundary would have to be displaced if the entire flow was replaced by a similar frictionless flow both having the same mass flow at any flow cross-section.

Since the incident shock wave was brought to rest by using a Galilian transformation, the boundary layer displacement thickness in the present case is negative (see figure 11).

In reality the flow associated with the RR is viscous, therefore solving it as an

inviscid flow (figure 12a) is inadequate. If one is to use the inviscid conservation equations, the geometrical boundary must be corrected in order to account for the viscous effects. One possible way is by displacing the flow boundary (wall) according to the boundary layer displacement thickness. The resulting flow field is shown in figure 12b. As can be seen the boundary condition for RR is no longer $\theta_1 + \theta_2 = 0$. The boundary condition that the flow obeys behind the reflected shock wave is $\theta_1+\theta_2=\alpha$ where $\alpha\neq 0$. Therefore, at transition

$$\theta_1 + \theta_{2m} = \alpha \tag{30}$$

or alternately,

$$1 + \frac{\theta_{2m}}{\theta_1} = F_\delta \tag{31}$$

where F_δ - the boundary layer dissplacement thickness coefficient is defined as $F_\delta = \alpha/\theta_1$. Consequently, the solution of equations (2) to (10) with $F_P = 0$ and $\alpha \neq 0$ should provide the correct RR $\rightleftarrows$ MR transition for rough surfaces since it accounts for the surface roughness via the displacement thickness.

In the following the relation between F_δ and ϵ is developed. It is clear from figure 4 that for any given value of roughness size ϵ, the actual transiton points shift away from the "detachment" criterion transition line to smaller wedge angles. Thus, by selecting an appropriate value for F_δ the transition line could also be shifted to fit the experimental results.

The required values of F_δ for the given values of M_s and ϵ are listed in table 1. Inspecting these values indicates that in the range $1 < M_s \leq 2$ and $3.5 \leq M_s \leq 4.0$ F_δ is practically independent of M_s, i.e., F_δ can be assumed to depend soley on ϵ. Owing to this finding, in the subsequent discussions two separate ranges of M_s are considered, $1 < M_s \leq 2$ and $3.5 \leq M_s \leq 4$. The values chosen for F_δ for the range $1 < M_s \leq 2$ are shown in figure 13. It is apparent from figure 13 that the selected

values of F_δ reproduce the experimentally obtained RR $\rightleftarrows$ MR transitions for any roughness size ε fairly well.

The values of F_δ and α which reproduce the experimental results for the two ranges of the incident shock wave Mach number ranges are given in table 2.

The correlations between F_δ and ε, based on the experimental results shown in figure 13, are:

for $1 < M_s \leq 2$

$$F_\delta = -600\,\varepsilon^2 + 38.6\,\varepsilon + 0.006 \qquad 0 < \varepsilon \leq 0.02 \text{ cm} \quad (32)$$

$$F_\delta = -4.17\,\varepsilon^2 + 3.08\,\varepsilon + 0.48 \qquad 0.02 \leq \varepsilon \leq 0.2 \text{ cm} \quad (33)$$

and for $3.5 \leq M \leq 4.0$

$$F = -9.45.45\,\varepsilon^2 + 37.13\,\varepsilon - 0.003 \qquad 0 < \varepsilon \leq 0.02 \text{ cm} \quad (34)$$

$$F = -1.39\,\varepsilon^2 + 2.47\,\varepsilon + 0.31 \qquad 0.02 \leq \varepsilon \leq 0.2 \text{ cm} \quad (35)$$

Obviously for a perfectly smooth surface ($\varepsilon = 0$) viscous losses can be ignored and therefore,

$$F_\delta = 0 \quad (36)$$

Equations (32) to (35) along with the experimentally deduced values of F_δ and ε are plotted in figure 14.

In summary, the procedure for employing the boundary layer displacement thickness model is as follows: for a given value of roughness height - ε (in cm) and incident shock wave Mach number - M_s, the value of F_δ is calculated from the appropriate correlation [equations (32) to (36)]. Then the conservation equations [(2) to (10)] are solved using the obtained value of F_ε (with $F_p = 0$). Besides its ability to reproduce the RR $\rightleftarrows$ MR transitions for rough surfaces, the proposed model (the boundary layer displacement thickness) can be justified on physical grounds. It will be shown in the following that for a given value of roughness height - ε, the slope of the boundary layer displacement thickness - δ^* at a specified point (which will be termed "the characteristic distance x_{char} ") is equal to the angle α which can be obtained from the model described earlier (which is based on experimental results) for the same value

of ε. (Recall that $\alpha = F_\delta/\theta_1$ is the angle between the flow direction behind the reflected shock wave and the real reflecting surface (see figure 12b)), i.e.,

$$\alpha = \tan^{-1} \left.\frac{d\delta^*}{dx}\right|_x \tag{37}$$

Intuitively, one might suggest that since the displacement starts at the reflection point G (figure 12b), equation (37) should be correct at $x_{char} = 0$. However, since $\tan^{-1} \left.\frac{d\delta^*}{dx}\right|_{x=0} = 90°$ and since a flow cannot follow a 90° turn instantaneously it appears that equation (37) must hold for $x_{char} \to 0$. Furthermore, following Shirouzo & Glass (1982) and Mireles (1983) it is preferable to use the average slope of the displaced boundary. Thus, equation (37) is replaced by:

$$\alpha = \tan^{-1} \left.\frac{\delta^*}{x}\right|_{x=x_{char}} \tag{38}$$

In order to proceed with the present analysis, an expression for the boundary layer displacement thickness $-\delta^*$ of a compressible viscous flow over rough flat plates is required. An appropriate expression is developed in appendix A. The obtained expression for δ^* (see equation A.17 in appendix A) is:

$$\frac{\delta^*}{x} = CG^{\frac{2(n-1)}{3n+1}} \left(\frac{T_m}{T_2}\right)^{\frac{3.2975n}{3n+1}} \left(\frac{\nu_2}{|v_2 - v_o| x}\right)^{\frac{2n}{3n+1}} \left(n+1 - \frac{T_2}{T_m}\right) \tag{39}$$

where C is a constant depending solely on n (equation A.18), n is the velocity profile exponent, which depends solely on the Reynolds number [Shames (1982), p. 281], G is the roughness characterizer [defined by equation (19)], T_2, v_2 and ν_2 are the flow temperature, the flow velocity and the kinematic viscosity behind the reflected shock wave respectively, T_m is the average temperature inside the boundary layer [defined by equation (A.8)] and V_o is the plate velocity on which the boundary layer develops.

Inserting equation (39) into equation (38) yields:

$$\alpha = \tan^{-1} \left\{ CG^{\frac{2(n-1)}{3n+1}} \left(\frac{T_m}{T_2}\right)^{\frac{3.2975n}{3n+1}} \left(\frac{\nu_2}{|v_2 - v_o| x}\right)^{\frac{2n}{3n+1}} \left(n+1 - \frac{T_2}{T_m}\right) \right\} \tag{40}$$

There are three unknown parameters in the right hand side of equation (40); they are:

1) the roughness characterizer - G which in the proposed model depends only on the roughness height - ε (this fact is yet to be proved),

2) the velocity profile exponent - n which according to Shames (1982) should decrease with increasing Reynolds numbers (this dependence is yet to be found),

3) the characteristic distance - x_{char}, which according to the present model should approach zero, i.e., $x_{char} \to 0$.

In the following these unknowns will be found. However, in order to do so we start by introducing an expression for the laminar sublayer thickness - δ_L (for details see appendix B):

$$\delta_L = G^{\frac{2}{n+1}} \left(\frac{\nu_2}{|v_2 - v_0|} \right)^{\frac{1}{n+1}} \delta^{\frac{n}{n+1}} Q^{-1/2} \qquad (41)$$

[appropriate expressions for Q and δ are developed in appendix A.]

For a hydraulically smooth surface G = 12.2468 (see the foregoing discussion) and from table 2, $\alpha = 4.63°$. Inserting these values as well as $n = \frac{1}{5}$ [see Martin (1975), Glass & Hall (1959)] into equation (39) yields,

$$x_{char} = 1.25 \times 10^{-6}$$

The mean free path of the flow behind the reflected shock wave at the conditions of the problem at hand is 10^{-6} cm. Thus it is seen that the characteristic length is of the order of the mean free path.

The mathematical definition of a hydraulically smooth surface can be easily obtained using equation (41). At x = 2 cm, which is half the length of our experimental models:

$$\delta_L \Big|_{x=2cm} = 0.00517 \text{ cm}$$

As mentioned earlier, a flow is considered as hydraulically smooth when the roughness height ε is smaller than the laminar sublayer thickness. Thus, for a hydraulically smooth surface

$$\varepsilon_{max} < \delta_L = 0.00517 \text{ cm} \tag{42}$$

It is also of interest to note that from equation (39)

$$\delta^*\big|_{x=2cm} = 0.00086 \text{ cm}$$

The obtained values for x_{char} and ε_{max} suggests two possible criteria for relating the roughness characterizer - G to the roughness height - ε.

Criterion A

Hypothesis: The above calculated value of x_{char} is independent of the roughness height - ε.

Verification: Using the constant value of x_{char} the values of G as a function of α (which depends on ε, table 2) were calculated. Using this procedure it was clear that for a given value of ε they are different values of G. This contradicts our basic requirement that G is independent of ε.

Conclusion: x_{char} depends both on the incident shock wave Mach number and the roughness height. Therefore, this criterion is incorrect.

Criterion B

Hypothesis: The value of $\frac{\delta^*}{\varepsilon}\big|_{x=2cm}$ is independent of the roughness height.

Verification: The value of $\frac{\delta^*}{\varepsilon}\big|_{x=2cm}$ for a hydraulically smooth surface can be easily obtained. Using the above calculated values of $\delta^*\big|_{x=2cm}$ and ε_{max}, one obtains:

$$\frac{\delta^*}{\varepsilon}\Big|_{x=2cm} = 0.166$$

(this is the minimum value since δ^* was divided by ε_{max}).

Assumption: The flow over a rough surface having $\varepsilon = 0.01$ cm belongs to the frictional transition flow zone. As mentioned earlier (equation 20)

$$G = 2.5\ (\ln G - \ln\beta)$$

and for the frictional transition flow zone (equation 14) $-2.2 \leq \ln\beta \leq 0.8$. Using an average value of $\ln\beta = 0.7$, results in:

$$G = 6.3848$$

Inserting this value of G together with $n = \frac{1}{5}$ into equation (39) results in:

$$\left.\frac{\delta^*}{\varepsilon}\right|_{x=2cm} = 0.176$$

Comparing this value (0.176) with the value obtained previously for a hydraulically smooth wedge (0.166) and recalling that the latter value is the minimum value for a hydraulically smooth wedge (these two values would be exactly equal if $\varepsilon = 0.0049$ cm which is smaller than ε_{max} was used for a hydraulically smooth surface), leads to the conclusion that $\frac{\delta^*}{\varepsilon}$ is independent of the roughness height ε.

Furthermore, equation (41) yields:

$$\left.\delta_L\right|_{x=2cm} = 0.0018 \text{ cm}$$

and since $\varepsilon = 0.01$ cm:

$$\left.\frac{\varepsilon}{\delta_L}\right|_{x=2cm} = 5.55$$

This value falls well within the range $1 < \frac{\varepsilon}{\delta_L} \lesssim 15$ which defines the frictional transition flow zone. Thus, the foregoing assumption is verified.

Let us now verify the argument that $\frac{\delta^*}{\varepsilon} = \text{const}$ in the range $1 \lesssim M_s \lesssim 2$ as well. For a hydraulically smooth surface and $M_s = 1.5$ one obtains:

$$\delta^*\Big|_{x=2cm} = 0.0059 \text{ cm}$$

Dividing this value by $\varepsilon = 0.0049$ cm (which is typical to a hydraulically wedge), results in:

$$\frac{\delta^*}{\varepsilon}\Big|_{x=2cm} = 1.204$$

Similarly, for a rough surface with $\varepsilon = 0.01$ cm, one obtains

$$\frac{\delta^*}{\varepsilon}\Big|_{x=2cm} = 1.224$$

The obtained values for $\frac{\delta^*}{\varepsilon}\Big|_{x=2cm}$ verify our hypothesis that $\frac{\delta^*}{\varepsilon}\Big|_{x=2cm}$ is practically independent of ε. Furthermore,

$$\frac{\varepsilon}{\delta_L}\Big|_{x=2cm} = 1.25$$

This value again verifies our earlier assumption that the flow over a plate with $\varepsilon = 0.01$cm belongs to the frictional transition flow zone.

Conclusion: The hypothesis that $\frac{\delta^*}{\varepsilon}$ is independent of the roughness height - ε is correct.

Summary: For a given incident shock wave Mach number

$$\frac{\delta^*}{\varepsilon}\Big|_{x=2cm} = \text{constant}$$

In the framework of the present study:

$$\frac{\delta^*}{\varepsilon}\Big|_{x=2cm} = 1.224 \text{ for } 1 < M_s \lesssim 2 \qquad (42)$$

$$\left.\frac{\delta^*}{\varepsilon}\right|_{x=2cm} = 0.176 \text{ for } 3.5 \leq M_s \leq 4.0 \qquad (43)$$

The velocity exponent - n

Using the foregoing criterion, the value of the velocity exponent - n (equation 23) can be calculated for any given incident shock wave Mach number.

Martin (1957) showed that in the range $1 < M_s \leq 2$ the value of $n = \frac{1}{5}$ fits experimental results best. Glass & Hall (1959) also arrived at this conclusion. Based on these studies the value $n = \frac{1}{5}$ was chosen for the range $1 < M_s \leq 2$. Schlichting (1962) claimed that the value of n decreases when the flow (shock) Mach number increases. The appropriate value of n for any shock Mach number can be calculated using the fact that the roughness characterizer is independent of the shock Mach number. For example, for the range $3.5 \leq M_s \leq 4.0$ one should solve the equation

$$G\left(\varepsilon=\varepsilon_1,\ M_s=3.75,\ n=?,\ \left.\frac{\delta^*}{\varepsilon}\right|_{x=2cm} = 0.176\right) =$$

$$G\left(\varepsilon=\varepsilon_1,\ M_s=1.5,\ n=\frac{1}{5},\ \left.\frac{\delta^*}{\varepsilon}\right|_{x=2cm} = 1.224\right).$$

The solution of this equation results in n = 0.1935, in agreement with the requirement that for $M_s > 2$, $n < 0.2$. The change in the obtained value of n is not too large. Nevertheless, the present procedure provides a method for calculating the value of n for any incident Mach number. It is expected that when the incident shock wave Mach number increases to higher values, n will be further reduced below 0.2.

The roughness characterizer - C

Using the values F_δ given in table 2 for any value of roughness height, together with the appropriate criterion [equations (42) or (43)] and equation (39), enabled us to find the values of the roughness characterizer - C for a given roughness height - ε.

The obtained values are given in table 3. As can be seen, there are very slight differences between the obtained value of G for a specified value of ε. This fact complies with our earlier requirement that the roughness characterizer should be independent of the roughness height. The small discrepancy is probably due to the fact that the two criteria [equations (42) and (43)] were established for $M_s = 1.5$ and $M_s = 3.75$, while the values in table 3 are for $M_s = 1.495 \pm 0.015$ and $M_s = 3.74 \pm 0.15$.

The average values of G (given in table 3) were fitted against ε to result in

$$G = \frac{0.062}{\varepsilon} + 0.252 \qquad (44)$$

(ε in cm). This curve, as well as the (G-ε) values given in table 3, are shown in figure 15. It is worthwhile to note that this expression complies with the physical requirement that the value of the shear stress $-\tau_w$ (equation A.14) increases as the roughness height ε increses. Note also that for a perfectly smooth surface (ε=0), equation (44) results in $G \to \infty$ and from equation (A.14) one gets for this case ($G \to \infty$) $\tau_w \to 0$ as expected.

A Further Check of the Displacement Thickness Model

The boundary layer displacement thickness model was based on experimental data obtained for ε = 0.01, 0.02, 0.08 and 0.2 cm. In order to consolidate the findings additional experiments with ε = 0.04 cm were performed.

The RR $\rightleftarrows$ MR transition lines obtained by the present model for the ranges $1 < M_s \leq 2$ and $3.5 \leq M_s \leq 4.0$ together with the experimentally measured transition data are plotted on figure 16. The von Neumann "detachment" transition line is also shown in figure 16. It is clearly seen that the predictions of the present model are much better than that of the von Neumann "detachment" criterion. As expected, in the range $1 \leq M_s \leq 2$ excellent agreement is obtained at the center of this range ($M_s = 1.5$). The predictions of the present model for the range $3.5 \leq M_s \leq 4.0$ are not as good as those obtained for the range $1 < M_s \leq 2$. However, they are far better than the

predictions of the "detachment" criterion.

Conclusions

Two models for predicting the effect of the surface roughness on the RR $\rightleftarrows$ MR transition in the (M_s, θ_w)-plane were developed. They are:

1) the pressure loss model, and

2) the boundary layer displacement thickness model,

These two models suggest alternative ways to account for viscous effects when treating the RR $\rightleftarrows$ MR transition.

In order to develop the boundary layer displacement thickness model, an expression for the boundary layer thickness of a compressible flow over rough, moving flat plates was developed. Using this expression, appropriate expressions for both the boundary layer displacement thickness and the laminar sublayer thickness were derived.

While developing the boundary layer displacement thickness the following facts were established.

1) A hydraulically smooth surface is a surface for which the roughness height $\varepsilon < 0.00517$ cm .

2) The roughness characterizer $G = \frac{v \delta_L}{\nu}$ is independent of the incident shock wave Mach number.

3) The value of $\left.\frac{\delta^*}{\varepsilon}\right|_{x=2cm}$ does not depend on the roughness height.

4) The characteristic distance - x_{char} increases with decreasing incident shock wave Mach number, and increasing roughness height.

5) In addition, a method by which the velocity exponent - n can be determined for any incident shock wave Mach number was presented.

Both models reproduce the experimental results quite well.

Appendix A - The Boundary Layer Displacement Thickness δ^*

The origin of the coordinate system is moving with the reflection point G along the wedge at a constant velocity $v_o = u_s/\cos\theta_w$ (u_s is the incident shock wave velocity in th laboratory frame of reference and θ_w is the wedge angle, see figure 12b). In this frame of reference the flow in state (0) is moving towards the incident shock wave (which is now stationary) with a velocity v_o (the angle of incidence between this flow and the shock wave is $\phi_o = 90 - \theta_w$). The wall, which in a laboratory frame of reference is at rest, is also moving now with the velocity $u_w = v_o$. The flow in state (2), which initially had an induced velocity $u_2(y)$, is now moving with the velocity $v_2(y) = [u_s - u_2(y)]/\cos\theta_w$. Therefore, in the considered frame of reference δ^* should be calculated for a flow velocity $v_2(y)$ over a moving inclined flat plate having a velocity v_o in the same direction of $v_2(y)$.

For turbulent incompressible boundary layer flows two different approaches are frequently used (both are semi-empirical): they are the mixing length of Prandtl and the von-Karman momentum integrals (see Shames, 1982, pp. 368). Since similar semi-empirical approaches are not available for compressible, turbulent boundary layer flows, it was suggested by Eckert (1954) and Mirels (1956) to adopt the approaches proposed for incompressible flows while adjusting them to account for compressibility effects. In the following a similar approach is adopted.

Prior to adjusting these approaches to the compressible case the differences between the incompressible and the compressible cases should be understood. While in the former the velocity and thermal boundary layers can be considered separately, in the latter they are coupled. This coupling arises from the fact that at high flow velocities the heat generated by friction and the temperature changes due to compressibility must be accounted for. Consequently, in the compressible case the following factors must be considered:

1) the Mach number,

2) the Prandtl number,

3) the viscosity dependence on temperature, and

4) the heat transfer from the flow to the solid surface.

The major assumptions upon which the present model is developed are:

1) the gas behaves as a perfect gas,

2) the flow is pseudo-steady and two-dimensional,

3) the boundary layer is turbulent from x = 0. This assumption is reasonable because,

   a) the Re number is very high. Therefore, [Martin (1957)] the boundary layer is laminar for a short distance only, and

   b) Schlichting (1962) showed that the surface roughness decreases the value of the critical Re number where transition takes place,

4) the gravitational forces can be neglected,

5) the pressure is constant throughout the entire field, i.e., $\frac{\partial P}{\partial x} = 0$ and $\frac{\partial P}{\partial y} = 0$, and

6) Blasius' semi-empirical results for the wall shear stress - τ_w in incompressible flows are applicable when the average temperature - T_m is used.

The wall shear stress - τ_w

In the following an expression for the wall shear stress in a compressible viscous flow over a moving rough flat plate is developed. The shear stress for an incompressible viscous flow over a rough stationary flat plate is (Mazor 1983):

$$\frac{\tau_w}{\rho_\infty} = u_\infty^2 \, G^{\frac{2(n-1)}{n+1}} \, Re_\delta^{-\frac{2n}{n+1}} \qquad (A.1)$$

where u_∞ and ρ_∞ are the flow velocity and density outside the boundary layer, G is the roughness characterizer $G = \frac{V_* \delta_L}{\nu}$ (V_* - shear velocity, δ_L - the laminar sublayer thickness, ν - kinematic viscosity), and

$$Re_\delta = \frac{u_\infty \delta}{\nu}$$

Inserting $n = \frac{1}{7}$ and C = 12.2468 (the value calculated previously for hydraulically smooth surfaces) in equation (A.1) yields:

$$\frac{\tau_w}{\rho_\infty} = 0.0233\, u_\infty Re^{-1/4} \qquad (A.2)$$

which is only 3.4% larger than Blasius' expression for incompressible flows over a smooth plate, i.e.,

$$\frac{\tau_w}{\rho_\infty} = 0.0225\, u_\infty Re^{-1/4}$$

In order to apply equation (A.2) to a compressible flow, the flow properties must be calculated for the average temperature inside the boundary layer - T_m. Consequently,

$$\frac{\tau_w}{\rho_m} = u_\infty^2\, G^{\frac{2(n-1)}{n+1}} \left(\frac{\nu_m}{u_\infty \delta}\right)^{\frac{2n}{n+1}} \qquad (A.3)$$

A similar approach was adopted by Tucker (1951), Eckert (1954), Bartz (1955) and Mireles (1956). By definition: $\nu_m = \mu_m/\rho_m$ and $\nu_\infty = \mu_\infty/\rho_\infty$, furthermore from the equation of state for a perfect gas: $\rho_m = P_m/(RT_m)$, $\rho_\infty = P_\infty/(RT_\infty)$ and from assumption 5, $P_\infty = P_m$. Inserting these expressions into equation (A.3) results in:

$$\frac{\tau_w}{\rho_\infty} = u_\infty^2\, G^{\frac{2(n-1)}{n+1}}\, Q \left(\frac{\nu_\infty}{u_\infty \delta}\right)^{\frac{2n}{n+1}} \qquad (A.4)$$

where

$$Q = \left(\frac{\mu_m}{\mu_\infty}\right)^{\frac{2n}{n+1}} \left(\frac{T_\infty}{T_m}\right)^{\frac{1-n}{n+1}} \qquad (A.5)$$

Equation (A.4) differs as expected from equation (A.1) by the term Q which

accounts for compressibility. In order to calculate Q, appropriate expressions for μ_m and T_m are required.

For nonpolar diatomic gases Mazor, Ben-Dor & Igra (1985) suggested,

$$\frac{\mu}{\mu_o} = \left(\frac{T}{T_o}\right)^{0.64874}$$

therefore

$$\frac{\mu_m}{\mu_o} = \left(\frac{T_m}{T_o}\right)^{0.64874} \tag{A.6}$$

Inserting this relation into equation (A.5) yields

$$Q = \left(\frac{T_\infty}{T_m}\right)^{\frac{1-2.2975n}{n+1}} \tag{A.7}$$

Eckert (1954) showed that T_m can be approximated by;

$$T_m = 0.5(T_w - T_\infty) + 0.22(T_r - T_\infty) \tag{A.8}$$

where T_w, T_∞ and T_r are the wall, the free stream and the recovery temperature, respectively.

The recovery temperature - T_r (which is equal to the wall temperature for the case when there is no heat transfer) can be calculated from [Schlichting (1962)]:

$$\frac{T_r}{T_\infty} = 1 + \left(\frac{u_w}{u_\infty} - 1\right) 2\,\frac{u_\infty^2\, Pr^{1/3}}{2T_\infty C_p} \tag{A.9}$$

where u_w and u_∞ are the wall and free stream velocities, respectively, Pr is the Prandtl number (calculated at T_r) and C_p is the specific heat capacity at constant pressure (calculated at T_r).

Mireles (1956) showed that equations (A.6) and (A.9) can be combined to result in:

$$\frac{T_m}{T_\infty} = \frac{5.56\,\frac{u_w}{u_\infty} - 0.28\left[1 + \left(\frac{u_w}{u_\infty}\right)^2\right]}{6\,\frac{u_w}{u_\infty} - 1} \tag{A.10}$$

Inserting equation (A.10) into equation (A.7) results in;

$$Q = \left\{ \frac{6\,\frac{u_w}{u_\infty} - 1}{5.56\,\frac{u_w}{u_\infty} - 0.28\left[1 + \left(\frac{u_w}{u_\infty}\right)^2\right]} \right\}^{\frac{1-2.2975n}{n+1}} \qquad (A.11)$$

As mentioned, in the present case the frame of reference is attached to the reflection point G (see figure 12b), thus: $u_w = v_o$, $u_\infty = v_2$, $\rho_\infty = \rho_2$, and $\nu_\infty = \nu_2$. Inserting these terms into equations (A.4) and (A.11) results in,

$$\frac{\tau_w}{\rho_2} = v_2^2\, G^{\frac{2(n-1)}{n+1}}\, Q\, \left(\frac{\nu_2}{v_2}\right)^{\frac{2n}{n+1}} \qquad (A.12)$$

and

$$Q = \left\{ \frac{6\,\frac{v_o}{v_2} - 1}{5.56\,\frac{v_o}{v_2} - 0.28\left[1 + \left(\frac{v_o}{v_2}\right)^2\right]} \right\}^{\frac{1-2.2975n}{n+1}} \qquad (A.13)$$

Equation (A.12) expresses the wall shear stress for a compressible flow over a rough flat plate. The compressibility is accounted for through Q and the roughness is accounted for through G. Additional correction is requried in order to use equations (A.12) and (A.13) for the problem at hand; i.e., to account for the fact that in the present case the flat plate is not stationary. This can easily be done by replacing v_2 in equation (A.12), by the relative velocity between the flow and the surface, $v_2 - v_o$. Carrying out this transformation finally results in:

$$\frac{\tau_w}{\rho_2} = (v_2 - v_o)^2\, G^{\frac{2(n-1)}{n+1}}\, Q\, \left(\frac{\nu_2}{|v_2 - v_o|\,\delta}\right)^{\frac{2n}{n+1}} \qquad (A.14)$$

The boundary layer thickness- δ

Inserting the velocity profile (equation 23) and the wall shear stress (equation A.14)

into von Karman's momentum integral for the case of zero pressure gradient, i.e., $\frac{\partial P}{\partial x} = 0$ [see Schlichting (1962)]

$$\tau_w = \frac{d}{dx} \int_0^\delta \rho[u^2 - (v_2 - v_o)u]dy$$

results in:

$$\frac{\delta}{x} = G \frac{2(n-1)}{3n+1} \left(\frac{T_m}{T_2}\right) \frac{3.2975n}{3n+1} Re_x - \frac{2n}{3n+1} \left[\frac{(3n+1)(2n+1)}{n}\right] \frac{n+1}{3n+1} \qquad \text{(A.15)}$$

where $Re_x = \frac{|v_2 - v_o|x}{\nu_2}$.

Equation (A.15) describes the boundary layer thickness for a compressible flow over a rough flat plate.

In the special case of an incompressible flow $\frac{T_m}{T_2} = 1$, over a smooth plate (C = 12.2468) when $n = \frac{1}{7}$ equation (A.15) reduces to

$$\frac{\delta}{x} = 0.3816\ Re_x^{-\frac{1}{5}}$$

The expression found in the literature for this case is ([see Schlichting (1962)]:

$$\frac{\delta}{x} = 0.376\ Re_x^{-\frac{1}{5}}$$

The difference between these two values is negligibly small (about 1.5%).

The boundary layer displacement thickness - δ^*

The boundary layer displacement thickness - δ^* can be calculated from [Schlichting (1962)]

$$\delta^* = \int_0^\delta \left(1 - \frac{\rho}{\rho_\infty} \frac{u}{u_\infty}\right) dy$$

Inserting the velocity profile (equation 23) into the above equation and carrying out the integration results in:

$$\delta^* = \delta \frac{1}{n+1} \left(n+1 - \frac{T_2}{T_m}\right) \qquad \text{(A.16)}$$

Inserting equation (A.15) into equation (A.16) finally yields:

$$\frac{\delta^*}{x} = C G^{\frac{2(n-1)}{3n+1}} \left(\frac{T_m}{T_2}\right)^{\frac{3.2975n}{3n+1}} \left(\frac{v_2}{\sqrt{v_2 - v_o}\, x}\right)^{\frac{2n}{3n+1}} \left(n+1 - \frac{T_2}{T_m}\right) \qquad (A.17)$$

where

$$C = \frac{1}{n+1} \left[\frac{(3n+1)(2n+1)}{n}\right]^{\frac{n+1}{3n+1}} \qquad (A.18)$$

Equation (A.17) describes the boundary layer displacement thickness for a compressible flow over a rough surface of a flat plate which moves with the velocity v_o relative to the free stream velocity v_2 .

Appendix B - The Laminar Sublayer Thickness - δ_L

The roughness characterizer G was defined (equation 19) as:

$$G = \frac{v_* \delta_L}{\nu} \tag{B.1}$$

where v_* the shear velocity is:

$$v_* = (\tau_w/\rho)^{\frac{1}{2}} \tag{B.2}$$

Inserting τ_w (equation A.14) into equation (B.2) results in:

$$v_* = (v_2 - v_0) G^{\frac{n-1}{n+1}} \left(\frac{\nu_2}{\delta |v_2 - v_0|}\right)^{\frac{n}{n+1}} Q^{\frac{1}{2}} \tag{B.3}$$

Using this value (equation B.3) in equation (B.1) and rearranging, yields:

$$\delta_L = G^{\frac{2}{n+1}} \left(\frac{\nu_2}{|v_2 - v_0|}\right)^{\frac{1}{n+1}} \delta^{\frac{n}{n+1}} Q^{-\frac{1}{2}} \tag{B.4}$$

δ and Q are defined in appendix A by equations (A.15) and (A.13), respectively.

List of References

Bartz, D.R., 1955, Trans. A.S.M.E., 77, 8, 1235.

Ben-Dor, G., 1978, UTIAS Re. 232, University of Toronto, Toronto, Canada.

Ben-Dor, G. and Glass, I.I., 1979, J. Fluid Mechanics, 92, 3, 459.

Bleakney, W. and Taub, A.H., 1949, Rev. Mod. Phys., 21, 584.

Eckert, E.R.G., 1954, Tech. Re. 54-70, Aero, Res. Lab., Wright Air Dev. Ctr., Wright Patterson A.F. Base, U.S.A.

Fletcher, C.H., 1950, Tech. Re. II-4, Dept. of Phys., Princeton Univ., N.J., U.S.A.

Henderson, L.F. and Lozzi, A., 1975, J. Fluid Mech., 68, 139.

Henderson, L.F. and Woolmington, J.P., 1983, 14th Int. Symp. on Shock Tubes and Waves, Sydney, Australia.

Hornung, H.G. and Taylor, J.R., 1982, J. Fluid Mech., 123, 145.

Hopf, L., 1923, ZAMM, 3, 329.

Law, C.K. and Glass, I.I., 1971, CASI Trans., 4, 1.

Martin, W.A., 1957, UTIAS Re. 47, University of Toronto, Toronto, Canada.

Mazor, G., 1984, M.Sc. Thesis in the Dept. of Mech. Eng., Ben-Gurion University of the Negev, Beer Sheva, Israel, (in Hebrew).

Mazor, G., Ben-Dor, G. and Igra, O., 1985, AIAA J., to be published.

Mireles, H., 1956, NACA TN 3712.

Mireles, H., 1983, private communication during his visit at the Dept. of Mech. Eng., Ben-Gurion Univ. of the Negev, Beer Sheva, Israel.

von Neumann, J., 1943, Explosive Res. Re. 12, Dept. of the Navy, Bureau of Ordnance, Washington, D.C., U.S.A.

von Neumann, J., 1963, Collected Works, Vol. 6, Pergamon Press.

Nikuradse, J., 1933, Forschungsheft 361.

Prandtl, L., 1925, ZAMM, 5, 136, Proc. 2nd Int. Cong. Appl. Mech., Zurich (1926).

Schlichting, H., 1962, Boundary Layer Theory , 4th Ed., McGraw-Hill Book Co., pp. 475-563.

Shames, I.H., 1982, Mechanics of Fluids , 2nd Ed., McGraw-Hill Book Co.

Shirouzu, M. and Glass, I.I., 1982, UTIAS Re. 264, University of Toronto, Toronto, Canada.

Smith, L.G., 1945, OSRD Re. 6271 or NORC Re. A2350.

Takayama, K., Gotoh, J. and Ben-Dor, G., 1981, Shock Tubes and Waves , edited by C.E. Treanor and J.G. Hall, S.U.N.Y. Press, Albany, N.Y., USA.

Taub, A.H., 1947, Rev. Mod. Phys., 21, 51.

Tucker, M., 1951, NACA TN 2337.

White, D.R., 1951, Tech. Re. II-10, Dept. of Phys., Princeton Univ., N.J., U.S.A.

Figure Captions

Figure 1: Illustration of four possible shock wave reflections. (Interferograms are on the left and explanatory diagrams on the right):
a) regular reflection (RR) θ_w = 60°, M_s = 4.68.
b) single-Mach reflection (SMR) θ_w = 10°, M_s = 4.72.
c) complex-Mach reflection (CMR) θ_w = 20°, M_s = 6.90.
d) double-Mach reflection (DMR) θ_w = 40°, M_s = 3.76.
The test gas is nitrogen at $P_o \simeq 15$ torr and $T_o \simeq 300$K.
(I, I_1 - incident shock waves, R, R_1 - reflected shock wave, M, M_1 - Mach stems, S, S_1 - slipstreams, T, T_1 - triple points, K-K_{ink} χ , χ_1 - triple point trajectory angles, (0)-(5) - thermodynamic states. The interferograms were taken in the UTIAS 10 x 18 cm Hypervelocity Shock Tube.

Figure 2: Wave configuration of a regular reflection.
I - incident shock wave, R - reflected shock wave, P - reflection point, U_s - incident shock wave velocity, ϕ - angle of incidence, θ- deflection angle, θ_w - wedge angle.

Figure 3: Comparison between the von Neuman "detachmen" criterion and the experimental results on RR $\rightleftarrows$ MR transition over smooth wedges in pseudo-steady flows. The disagreement is known as the von Neuman paradox.

Figure 4: Experimental results of the RR $\rightleftarrows$ MR transition over rough wedges. ε - roughness height, and the "detachment" criterion.

Figure 5: a) Schematic illustration of the type of roughness used in the experimental study.

b) The test section and the adjustable test model.

Figure 6: a) SMR over an ε = 0.02 cm wedge.
b) RR over an ε = 0.02 cm wedge.
c) SMR over an ε = 0.2 cm wedge.
d) RR over an ε = 0.2 cm wedge.

Figure 7: Illustration of the method used to obtain the RR $\rightleftarrows$ MR transition wedge angle ($\theta_{w,tr}$) [ξ - inverse pressure ratio (P_o/P_1) across the shock wave].

Figure 8: Schematic illustration of the boundary layer structure over a flat plate.

Figure 9: The predictions of the pressure loss model against the experimental result for various sizes of roughness.

Figure 10: The dependence of F_ε on ε.

Figure 11: Illustration of the boundary layer displacement thickness - δ^* in steady flows and pseudo-steady flows.
steady flow : (δ^* is positive)
a) velocity profile of the viscous flow
b) the equivalent inviscid velocity profile.

pseudo-steady flow : (δ^* is negative)
c) the unstedy viscous velocity profile
d) the pseudo-steady viscous velocity profile
e) the equivalent inviscid velocity profile

Figure 12: Schematic illustration of a viscous regular reflection at (a) and the equivalent inviscid regular reflection at (b).

Figure 13: The predictions of the boundary layer displacement thickness model against the experimental results for various sizes of roughness.

Figure 14: The dependence of F_δ on ε.

Figure 15: The dependence of the roughness characterizer C on ε.

Figure 16: The detachment criterion of von Neuman and the predictions of the boundary layer displacement thickness model for ε = 0.04 cm (in the two Mach number ranges) and experimental results of the RR $\rightleftarrows$ MR transition for ε = 0.04 cm.

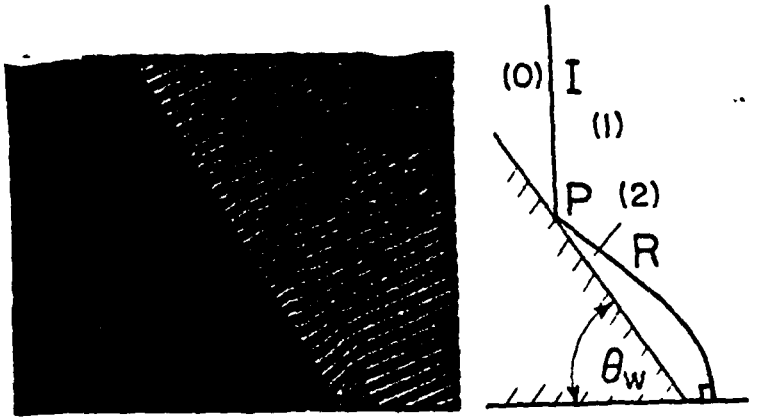

(a)

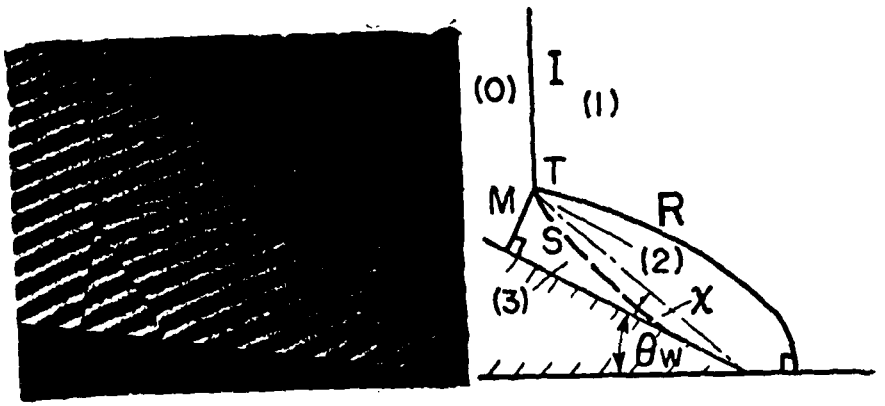

(b)

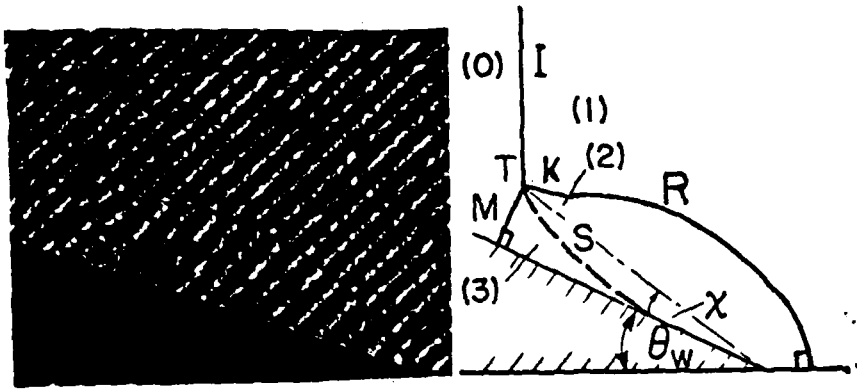

(c)

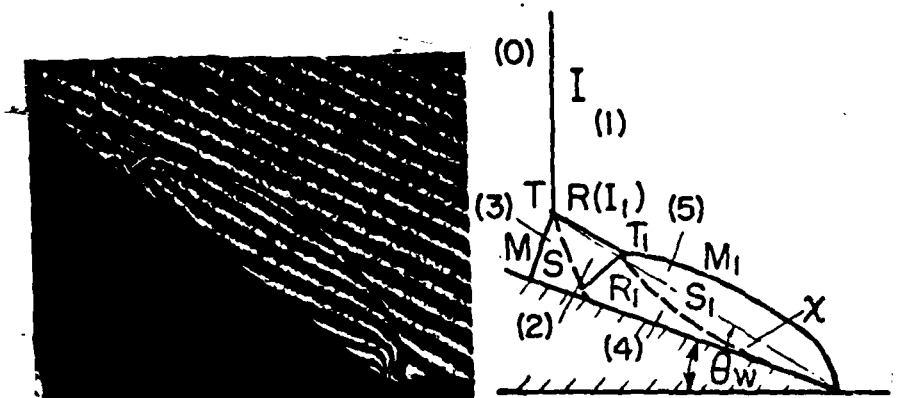

(d)

Figure 1

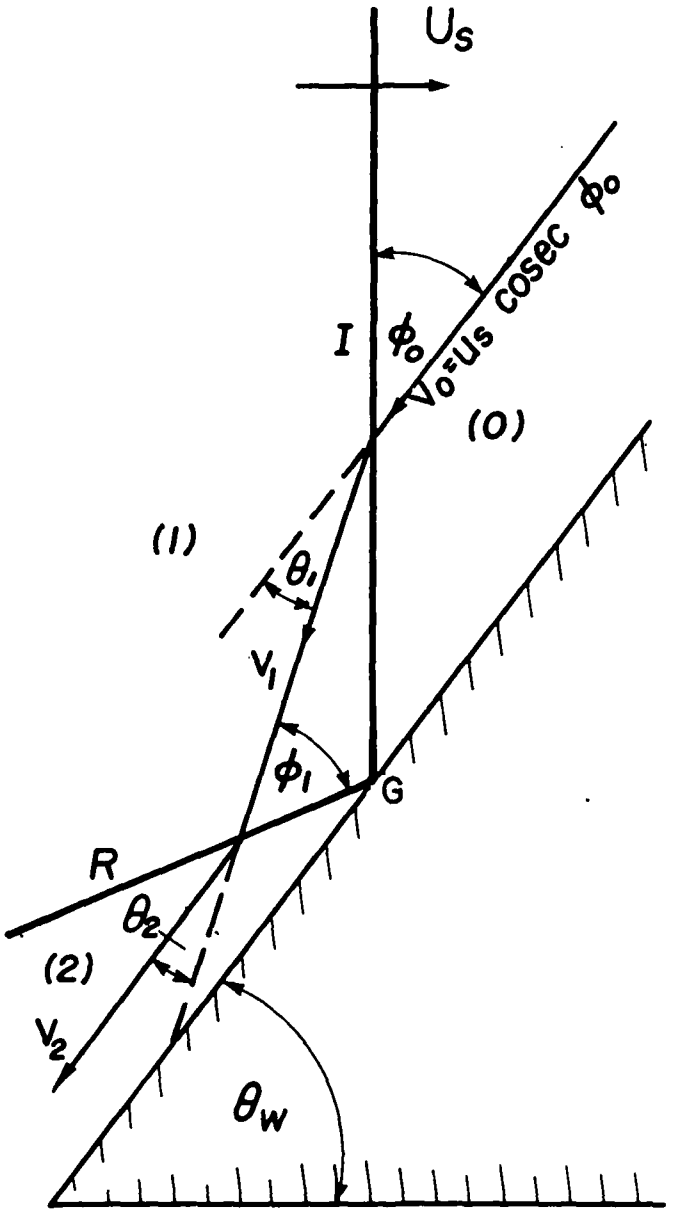
U_s
$V_0 = U_s \operatorname{cosec} \phi_0$
I
ϕ_0
(0)
(1)
θ_1
V_1
ϕ_1
G
R
θ_2
(2)
V_2
θ_w

Figure 2

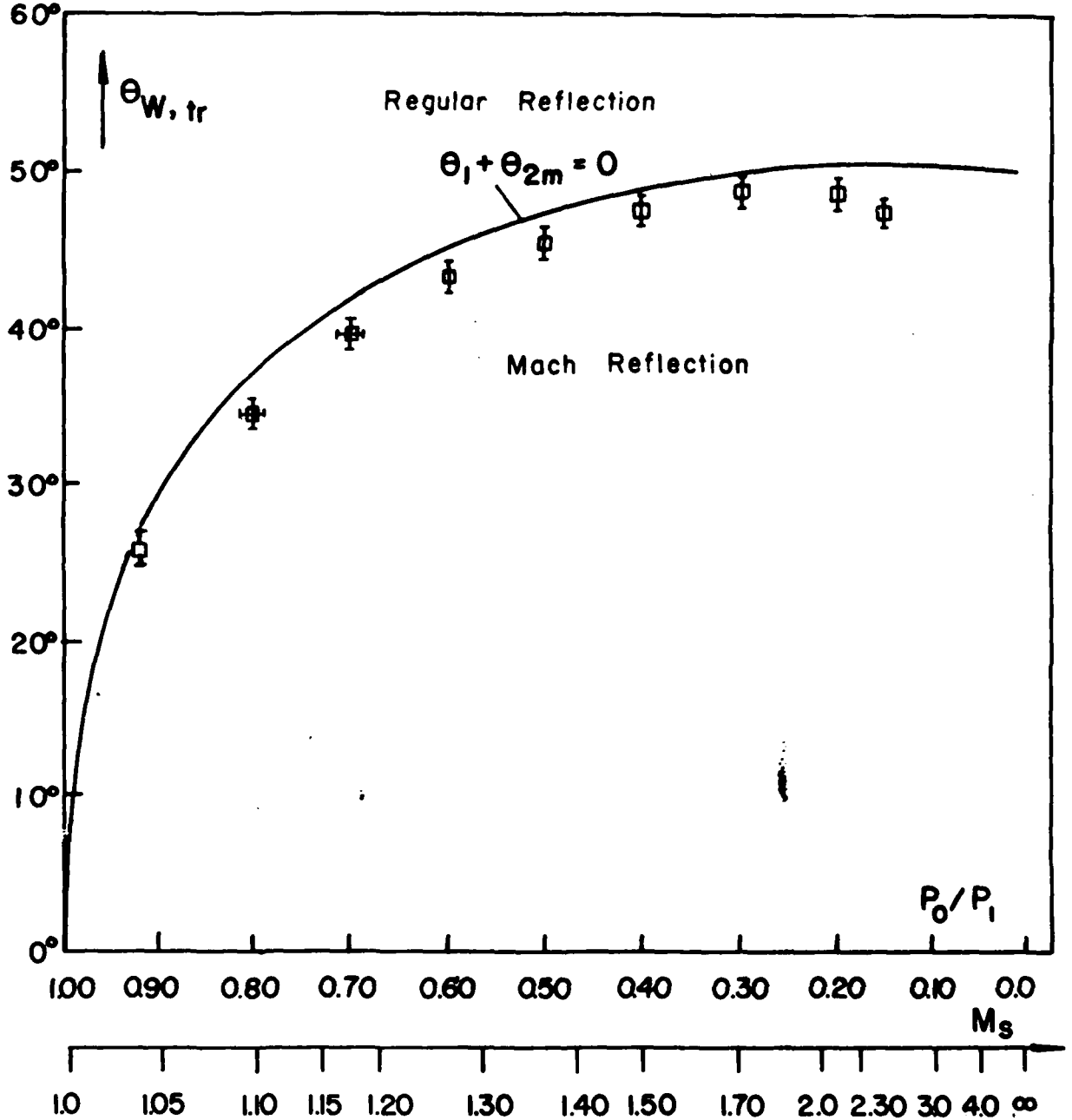
60°
50°
40°
30°
20°
10°
0°
$\theta_{W,tr}$
Regular Reflection
$\theta_1 + \theta_{2m} = 0$
Mach Reflection
P_0/P_1
1.00 0.90 0.80 0.70 0.60 0.50 0.40 0.30 0.20 0.10 0.0
M_S
1.0 1.05 1.10 1.15 1.20 1.30 1.40 1.50 1.70 2.0 2.30 3.0 4.0 ∞

Figure 3

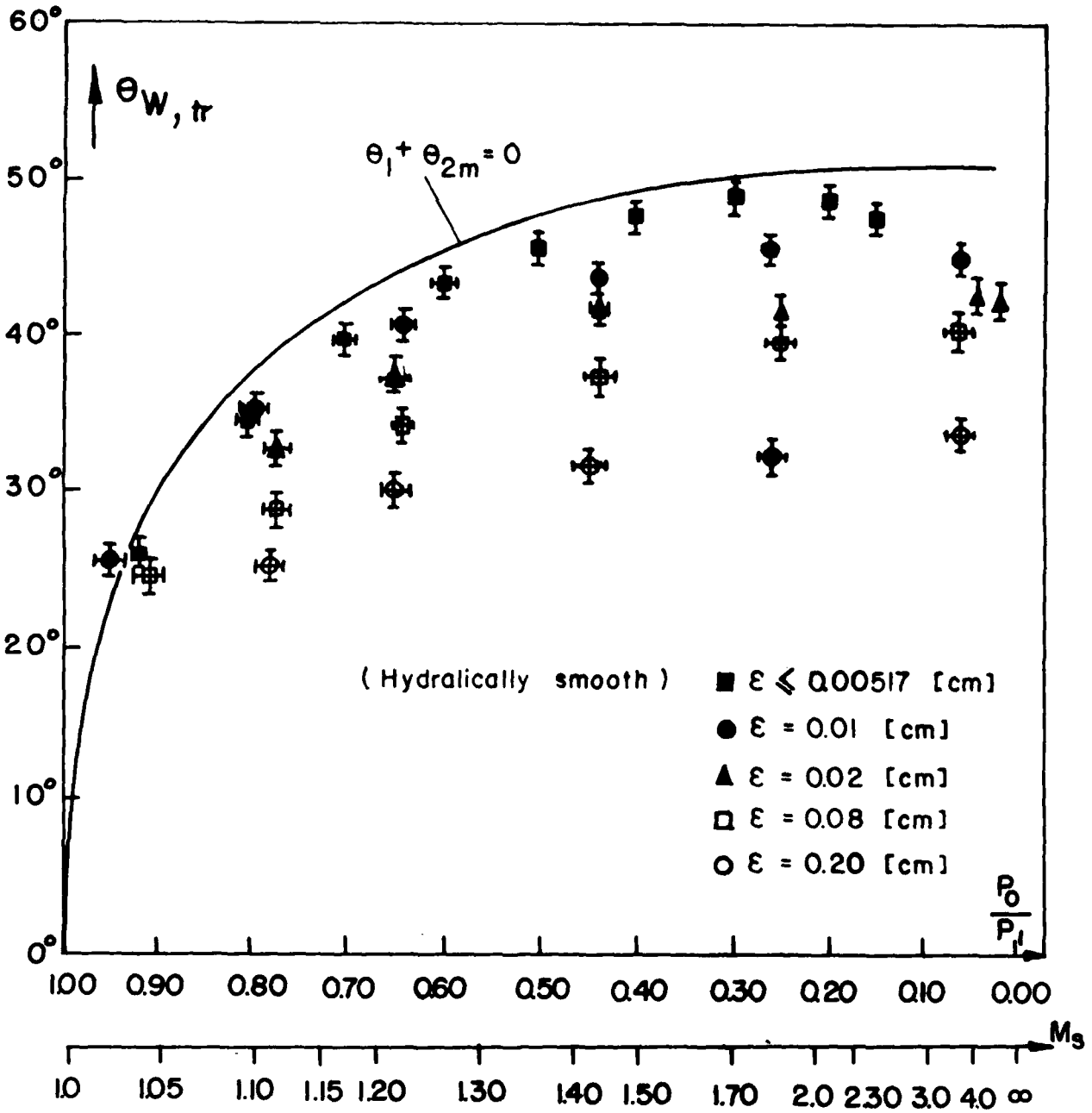
60°
50°
40°
30°
20°
10°
0°
$\theta_{W,tr}$
$\theta_1 + \theta_{2m} = 0$
(Hydralically smooth)
■ ε ≤ 0.00517 [cm]
● ε = 0.01 [cm]
▲ ε = 0.02 [cm]
□ ε = 0.08 [cm]
○ ε = 0.20 [cm]
$\frac{P_0}{P_1}$
1.00 0.90 0.80 0.70 0.60 0.50 0.40 0.30 0.20 0.10 0.00
M_s
1.0 1.05 1.10 1.15 1.20 1.30 1.40 1.50 1.70 2.0 2.30 3.0 4.0 ∞

Figure 4

ε[cm]	記号
0.01	I
0.02	II
0.08	III
0.2	IV

(a)

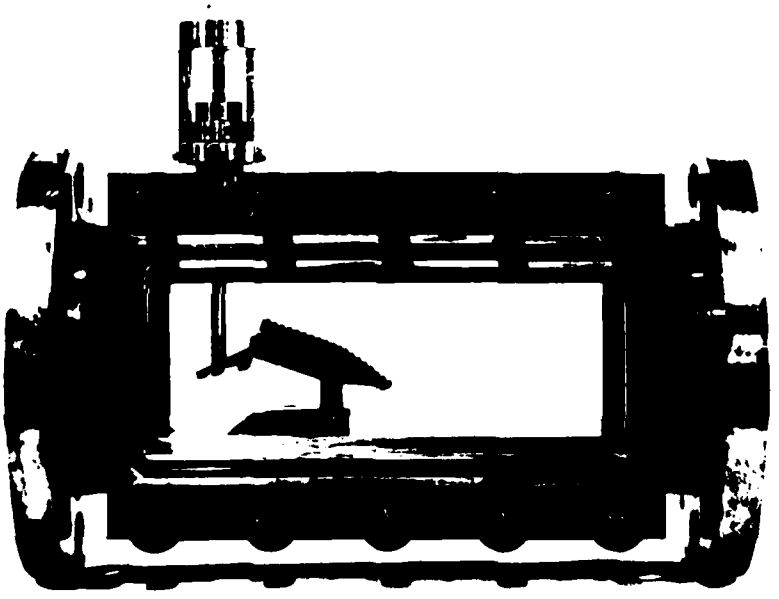

(b)

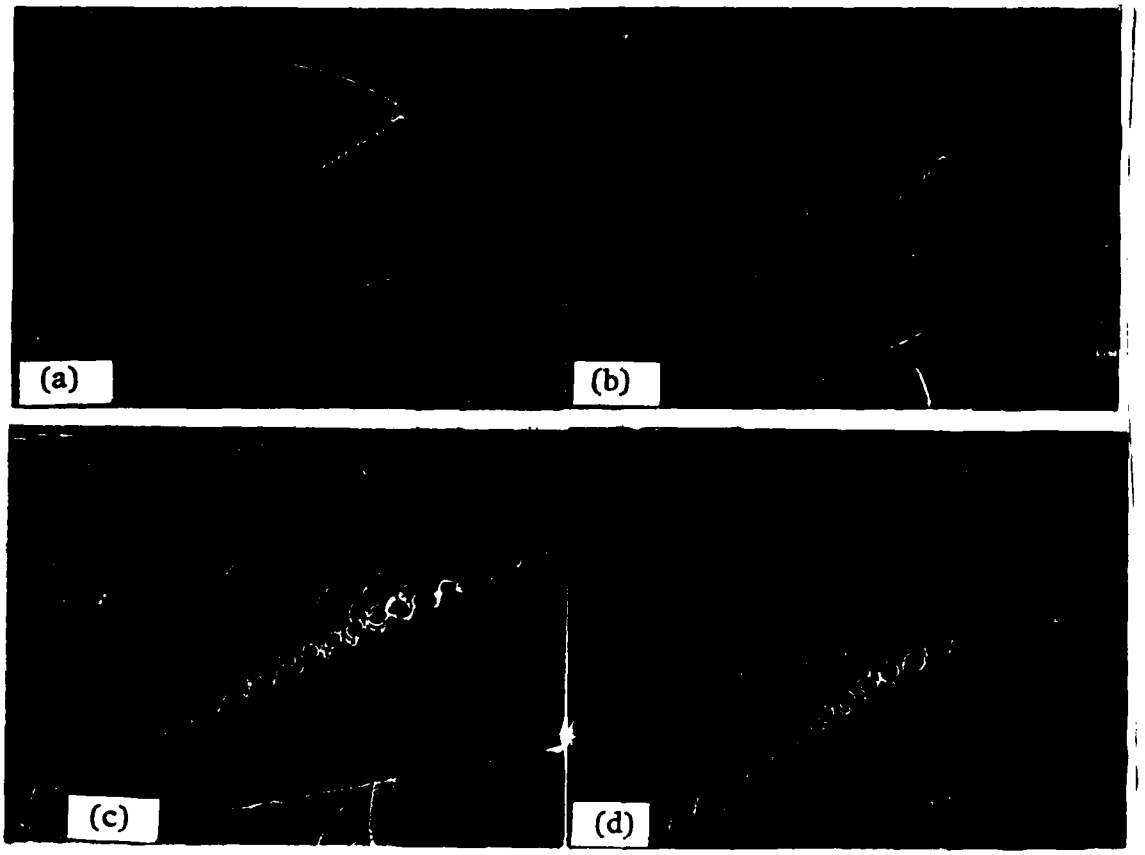

Figure 6

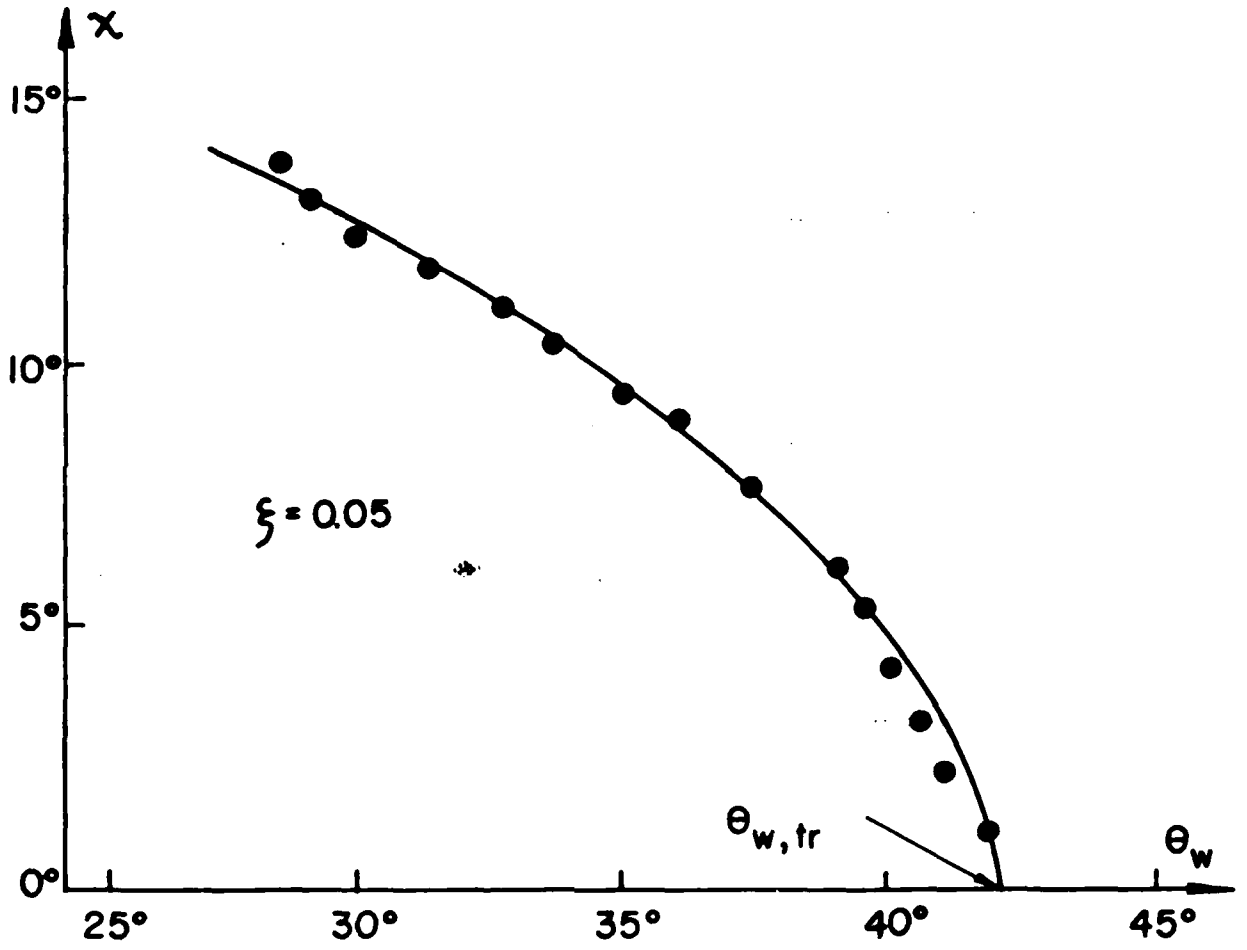

Figure 7

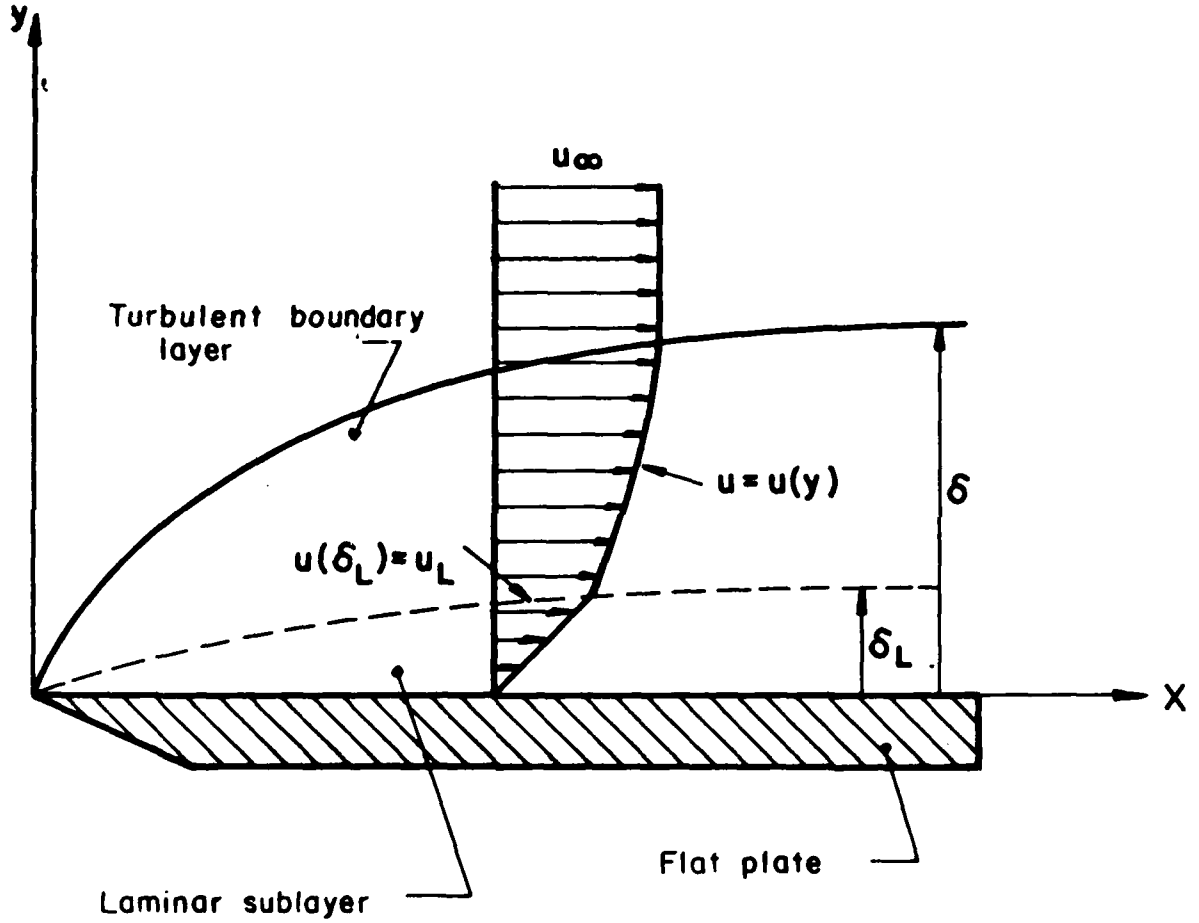
y
u_∞
Turbulent boundary layer
u = u(y)
δ
$u(\delta_L) = u_L$
δ_L
X
Laminar sublayer
Flat plate

Figure 8

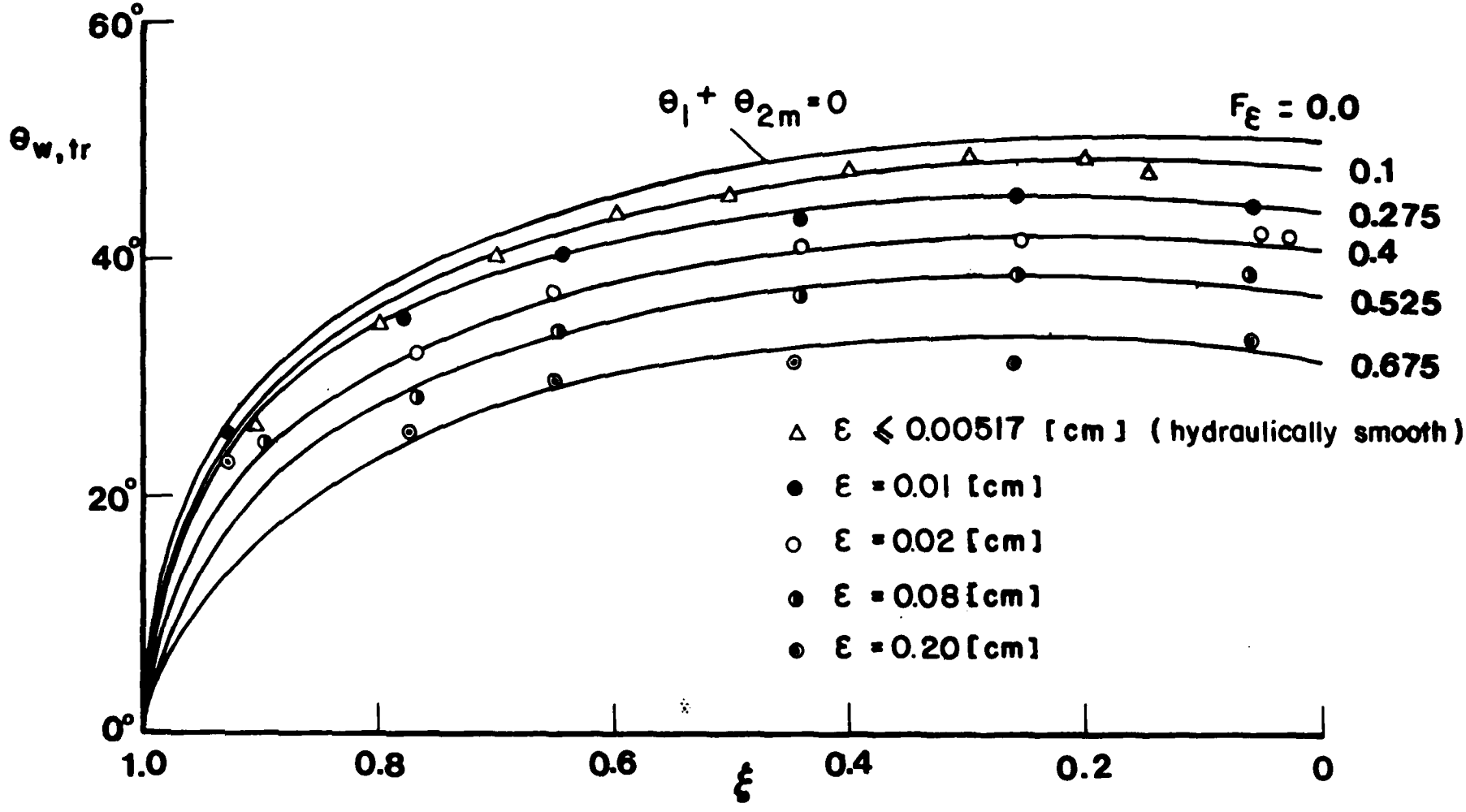
60°
40°
20°
0°
$\theta_{w,tr}$
$\theta_1 + \theta_{2m} = 0$
F_ε = 0.0
0.1
0.275
0.4
0.525
0.675
△ ε ≤ 0.00517 [cm] (hydraulically smooth)
● ε = 0.01 [cm]
○ ε = 0.02 [cm]
◐ ε = 0.08 [cm]
◐ ε = 0.20 [cm]
1.0
0.8
0.6
0.4
0.2
0
ξ

Figure 9

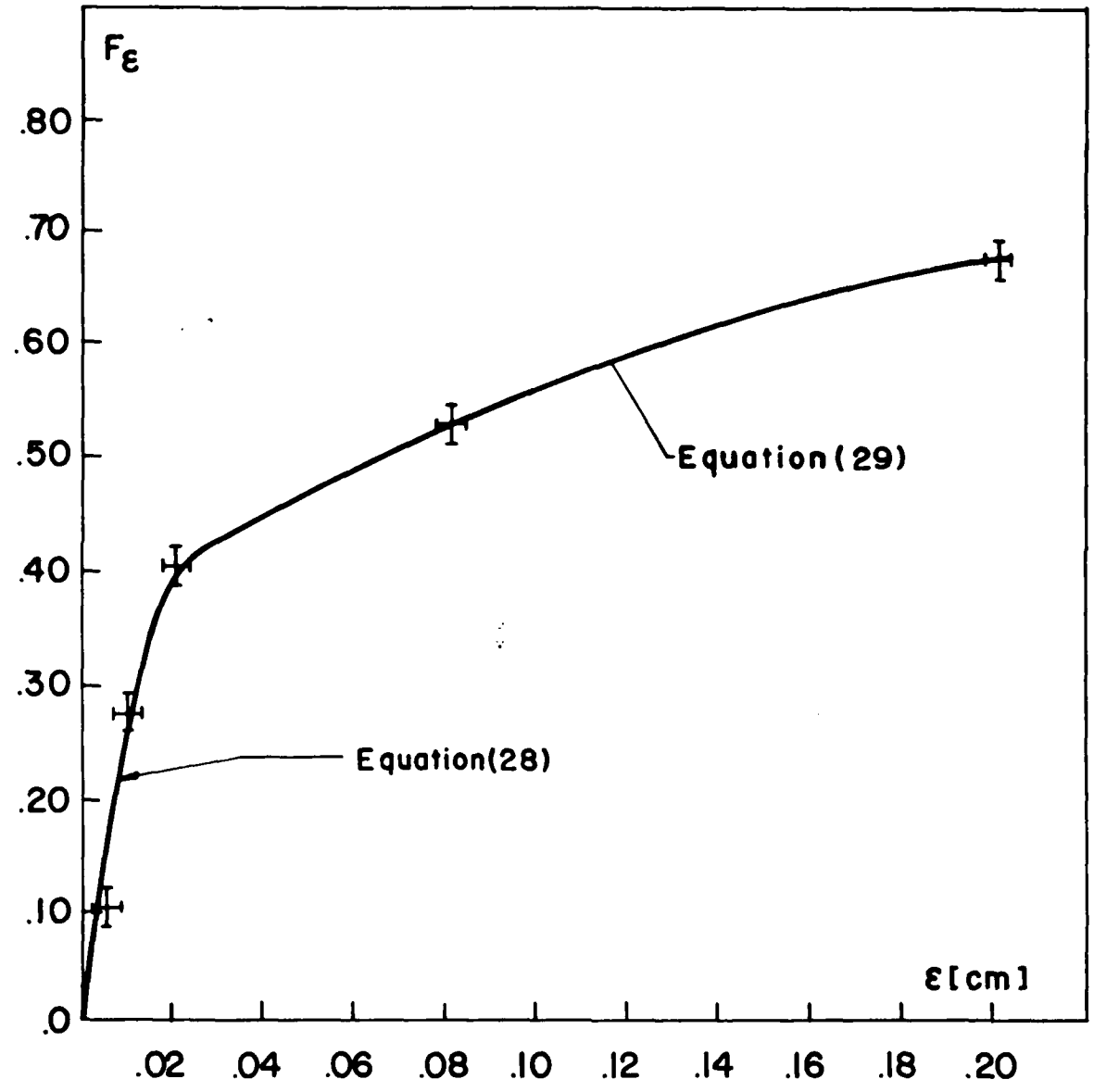
F_ε
.80
.70
.60
.50
.40
.30
.20
.10
.0
.02
.04
.06
.08
.10
.12
.14
.16
.18
.20
Equation(29)
Equation(28)
ε[cm]

Figure 10

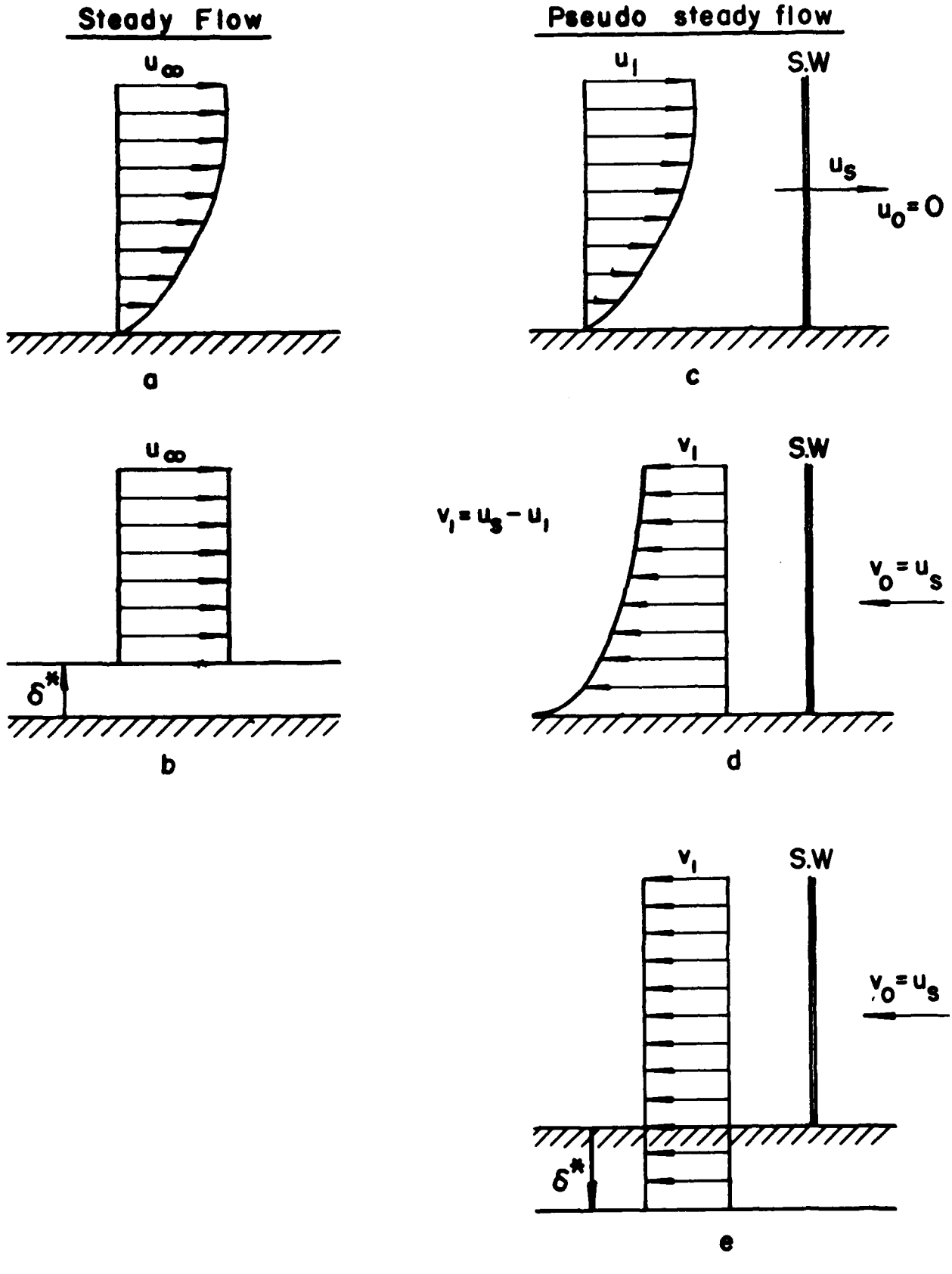
Steady Flow
u_∞
a
u_∞
δ^*
b
Pseudo steady flow
u_1
S.W
u_s
$u_0 = 0$
c
v_1
S.W
$v_1 = u_s - u_1$
$v_0 = u_s$
d
v_1
S.W
$v_0 = u_s$
δ^*
e

Figure 11

a.

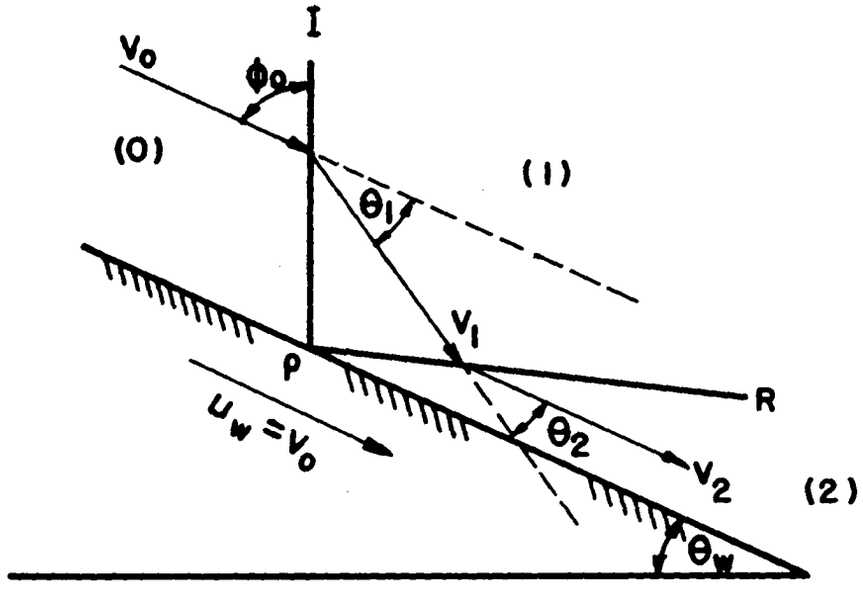
I
V_o
ϕ_o
(0)
(1)
θ_1
V_1
P
R
$u_w = V_o$
θ_2
V_2
(2)
θ_w

b.

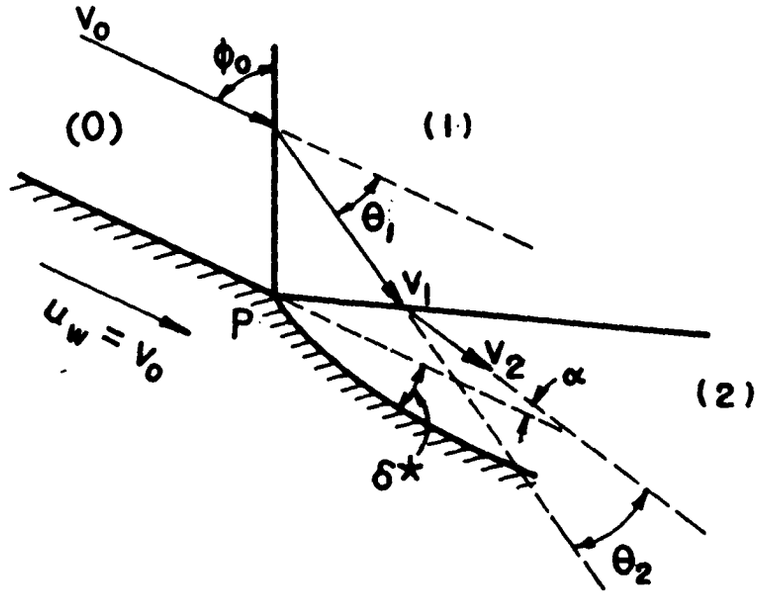
V_o
ϕ_o
(0)
(1)
θ_1
V_1
$u_w = V_o$
P
V_2
α
(2)
δ^*
θ_2

Figure 12

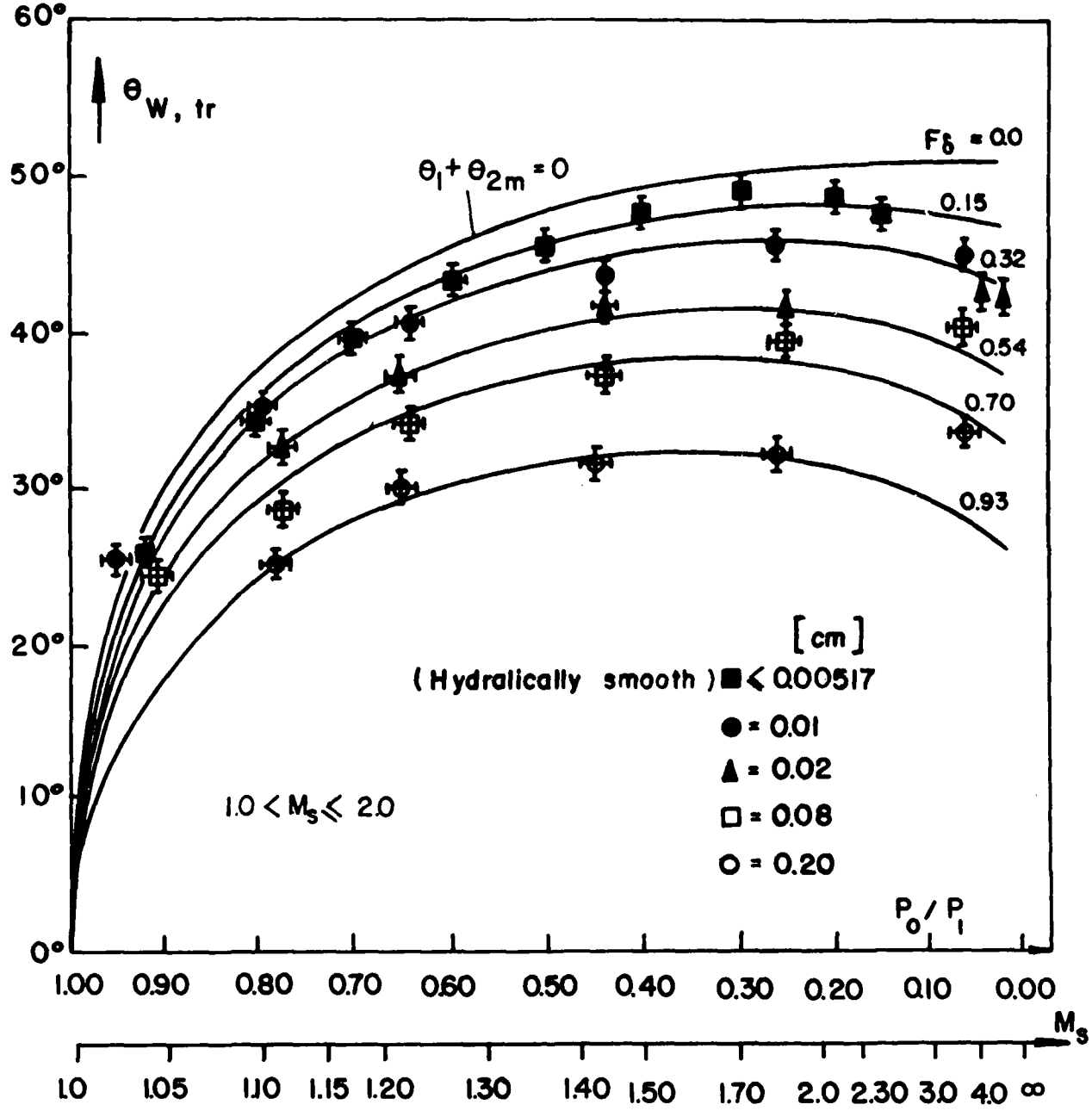
60°
50°
40°
30°
20°
10°
0°
θW, tr
θ1 + θ2m = 0
Fδ = 0.0
0.15
0.32
0.54
0.70
0.93
[cm]
(Hydralically smooth) ■ ≤ 0.00517
● = 0.01
▲ = 0.02
□ = 0.08
○ = 0.20
1.0 < Ms ≤ 2.0
P0 / P1
1.00 0.90 0.80 0.70 0.60 0.50 0.40 0.30 0.20 0.10 0.00
Ms
1.0 1.05 1.10 1.15 1.20 1.30 1.40 1.50 1.70 2.0 2.30 3.0 4.0 ∞

Figure 13

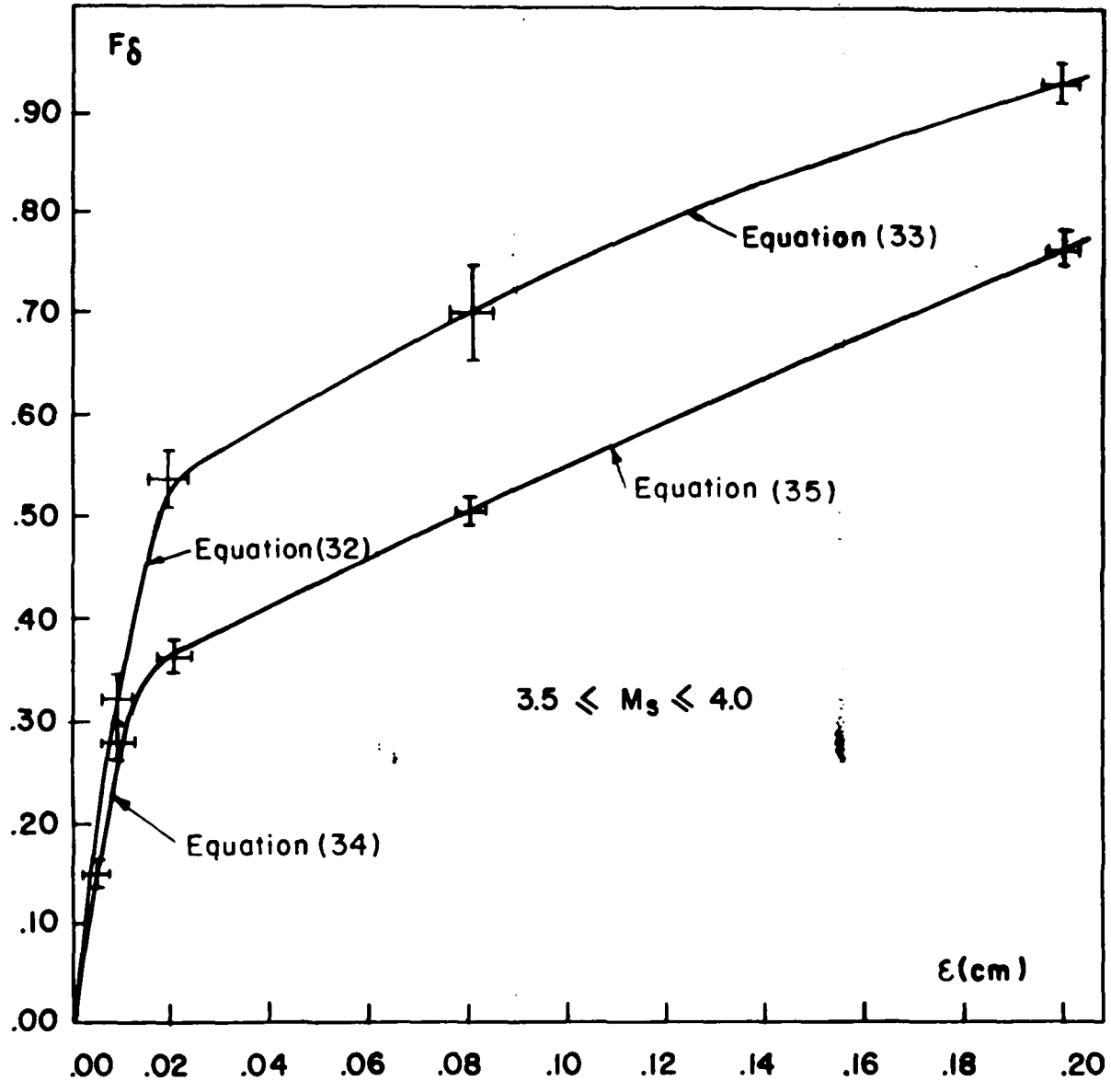
F_δ
.90
.80
.70
.60
.50
.40
.30
.20
.10
.00
.00
.02
.04
.06
.08
.10
.12
.14
.16
.18
.20
Equation (33)
Equation (35)
Equation(32)
Equation (34)
$3.5 \leqslant M_s \leqslant 4.0$
ε(cm)

Figure 14

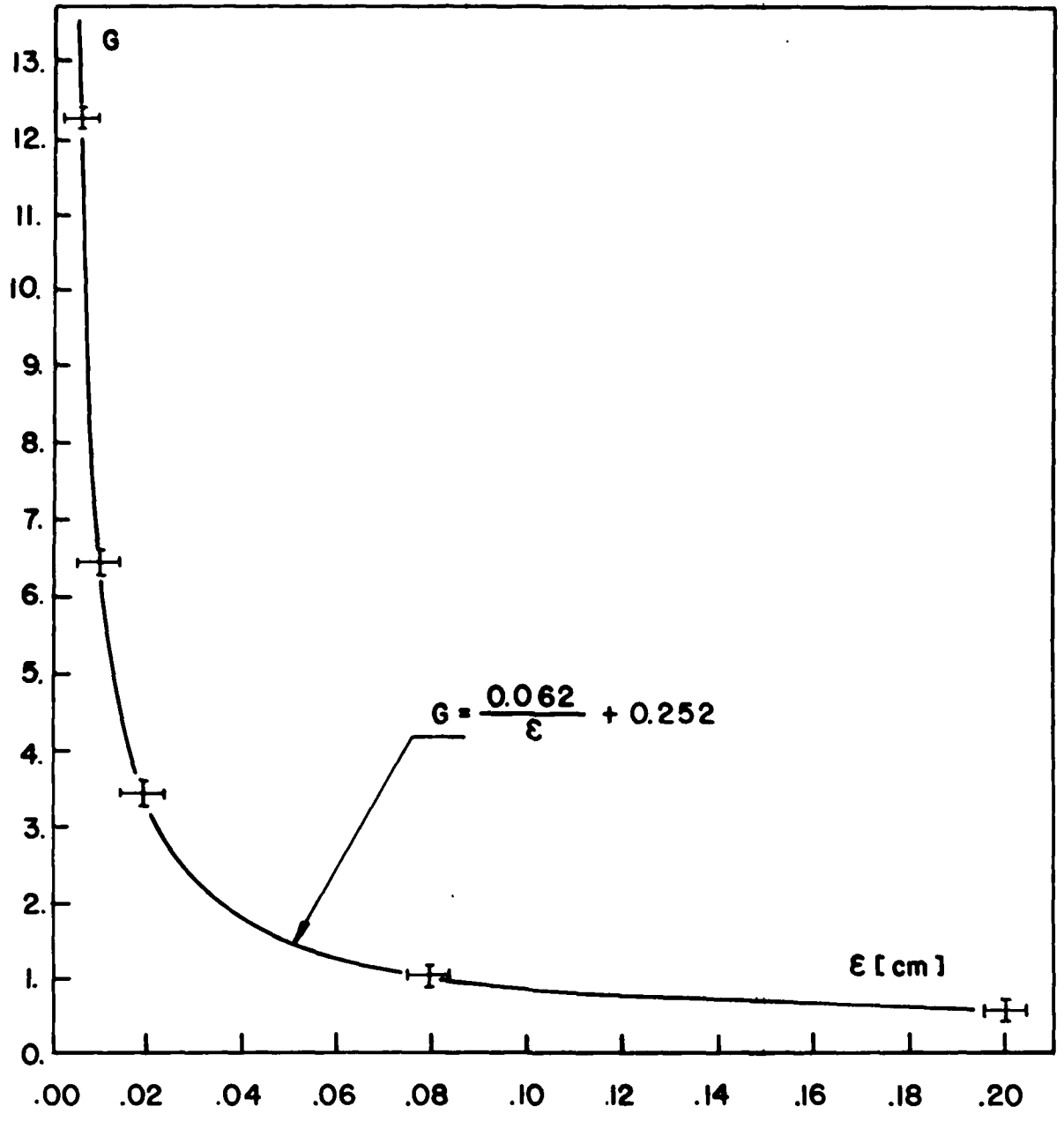
G
13.
12.
11.
10.
9.
8.
7.
6.
5.
4.
3.
2.
1.
0.
.00
.02
.04
.06
.08
.10
.12
.14
.16
.18
.20
G = 0.062/ε + 0.252
ε [cm]

Figure 15

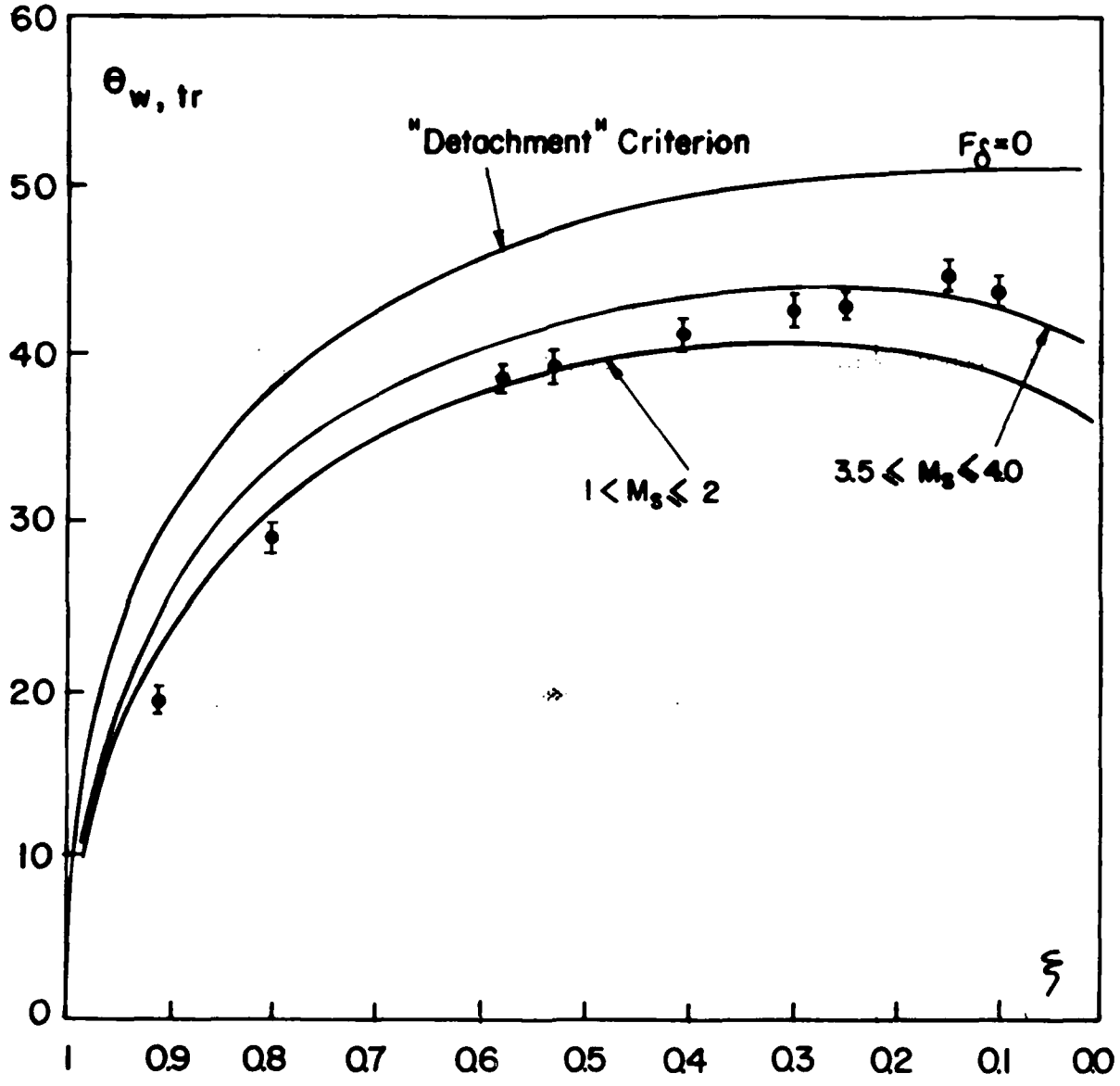
60
50
40
30
20
10
0
$\theta_{w,tr}$
"Detachment" Criterion
$F_\delta=0$
$1<M_s\leq 2$
$3.5\leq M_s\leq 4.0$
ξ
1
0.9
0.8
0.7
0.6
0.5
0.4
0.3
0.2
0.1
0.0

Figure 16

PART 2

The reflection of a planar shock wave over a liquid wedge.

Introduction

In order to have a better understanding of the blast reflection phenomenon over liquid surfaces such as seas or oceans an experimental study of the reflection of a planar shock wave over a water wedge was carried out.

Experiments

In order to get a planar shock wave reflecting over a water wedge a special shock tube has been designed and constructed in such a way that the whole tube could be tilted in a vertical plane. Using this technique, it was possible to adjust the shock tube inclination to obtain any desired water wedge angle. A schematic drawing of the tilted shock tube with the water wedge having an angle of θ_w as well as a planar shock wave reflecting from it as a Mach reflection is shown in figure 1.

A photograph of part of the inclined shock tube with the test section is shown in figure 2. A detailed view of the test section filled in with water is shown in figure 3.

The test gas throughout the experimental study was dry air. Both the test gas and the water were initially at room temperature.

Results

Two different incident shock wave Mach numbers were used with a variety of different wedge angles. The two Mach numbers were $M_1 = 1.475 \pm 0.015$ and $M_1 = 2.25 \pm 0.05$.

$M_i = 1.475 \pm 0.015$

Typical results for this case are shown in figures 4(a) to 4(d).

At $\theta_w = 44.3°$ the incident shock wave reflects over the water wedge as a regular reflection [figure 4(a)]. As the wedge angle is decreased regular reflection becomes impossible and the incident shock wave reflects over the water wedge as a single Mach reflection. Such a reflection is shown in figure 4(b) for $\theta_w = 25.8°$.

Further decrease in θ_w causes higher triple point trajectory angles. The reflection over a wedge with $\theta_w = 18.2°$ is shown in figure 4(c). Figure 4(d) illustrates the case of a glancing incidence ($\theta_w = 0$).

It is interesting to note that in all the above photographs a disturbance is seen to be propagating inside the water tank. Its front propagates along the air/water interface faster than the point of reflection of the regular reflection or the foot of the Mach stem.

$M_i = 2.25 \pm 0.05$

A typical regular reflection is shown in figure 5(a) for $\theta_w = 50.8°$. At lower wedge angles $\theta_w = 49.5°$ a double Mach reflection is obtained [figure 5(b)]. At even lower wedge angles $\theta_w = 25.8°$ the incident shock wave reflects as a single Mach reflection [figure 5(c)]. The disturbance propagating into the water is clearly seen in this set of experiments too.

The RR $\overset{\rightarrow}{\leftarrow}$ MR transition wedge angle

The RR $\overset{\rightarrow}{\leftarrow}$ MR transition wedge angles, θ_w^{tr}, were measured for both $M_i = 1.47$ and $M_i = 2.2$. The value of θ_w^{tr} was obtained by plotting the triple point trajectory angle χ as a function of the wedge angle θ_w for a given value of Mach number. Then the experimental results were extrapolated to get θ_w^{tr} at the point where $\chi = 0$. The present results are shown in figure 6.

The results are also shown in table 1. For the weaker incident shock wave the actual transition wedge angle is about 5° smaller than that predicted by the "detachment" criterion. For the stronger shock wave the agreement with the "detachment" transition wedge angle is surprisingly good. The agreement is better than that obtained over solid wedges.

At the present a detailed study of the reflection over a water wedge in the range $1 < M_i < 4$ is being carried out.

Conclusion

The reflection of a planar shock wave over a water wedge has been investigated using a tilted shock tube which was especially designed and constructed for this study.

The four well known types of reflection, namely RR, SMR, CMR and DMR, have all been observed over the water wedges.

The RR $\overset{\rightarrow}{\leftarrow}$ MR transition was investigated. Our early results indicate about a 5° disagreement with the "detachment" criterion at $M_i = 1.47$ and a surprisingly excellent agreement at $M_i = 2.2$. Further experiments are being carried out.

Table 1

Shock Wave Mach Number	Actual Transition Wedge Angle	"Detachment" Wedge Angle
1.47	43° ± 0.5°	48.7°
2.2	50.2° ± 0.5°	50.7°

APPENDIX - LIST OF EXPERIMENTS OVER A WATER WEDGE

θ_w	Ms
51.5	2.26
50.8	2.30
50.5	2.29
50.0	2.31
49.5	2.30
49.0	2.29
46.2	2.29
43.5	2.21
34.3	2.10
29.8	2.22
25.8	2.05
48.0	1.49
47.0	1.49
46.2	1.48
45.8	1.45
45.2	1.49
44.8	1.47
44.3	1.47
44.0	1.47
43.5	1.47
43.0	1.47
42.7	1.47
41.8	1.45
40.8	1.46
40.0	1.45
39.2	1.48
37.4	1.47
33.3	1.48
29.8	1.47
25.8	1.52
22.0	1.56
18.2	1.44
14.3	1.46
10.	1.46
7.2	1.46
2.3	1.42
0.	1.47

List of Figures

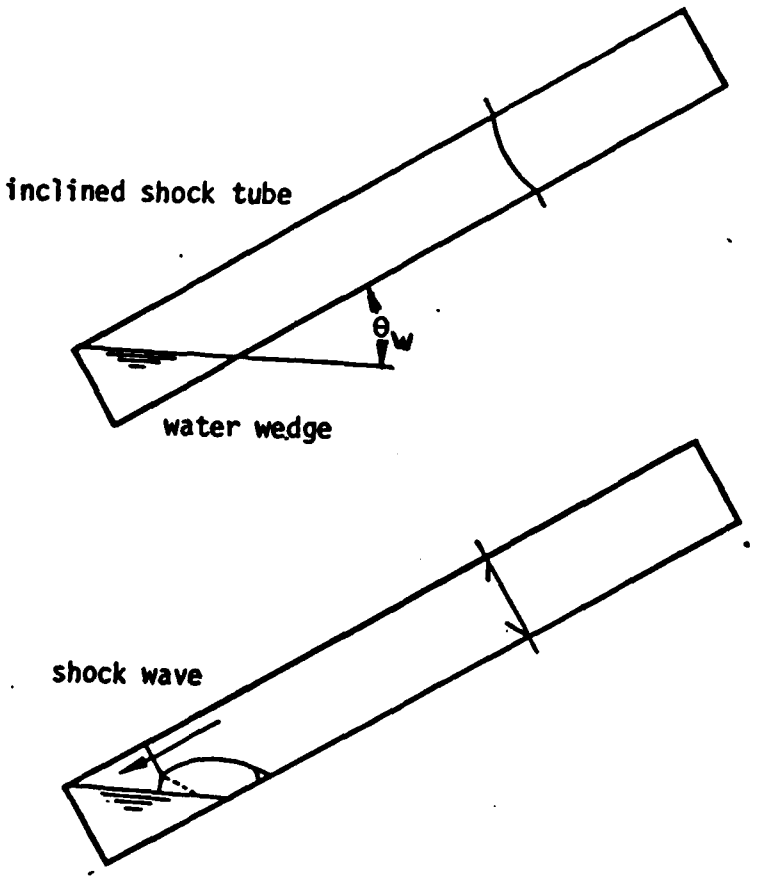

Fig. 1

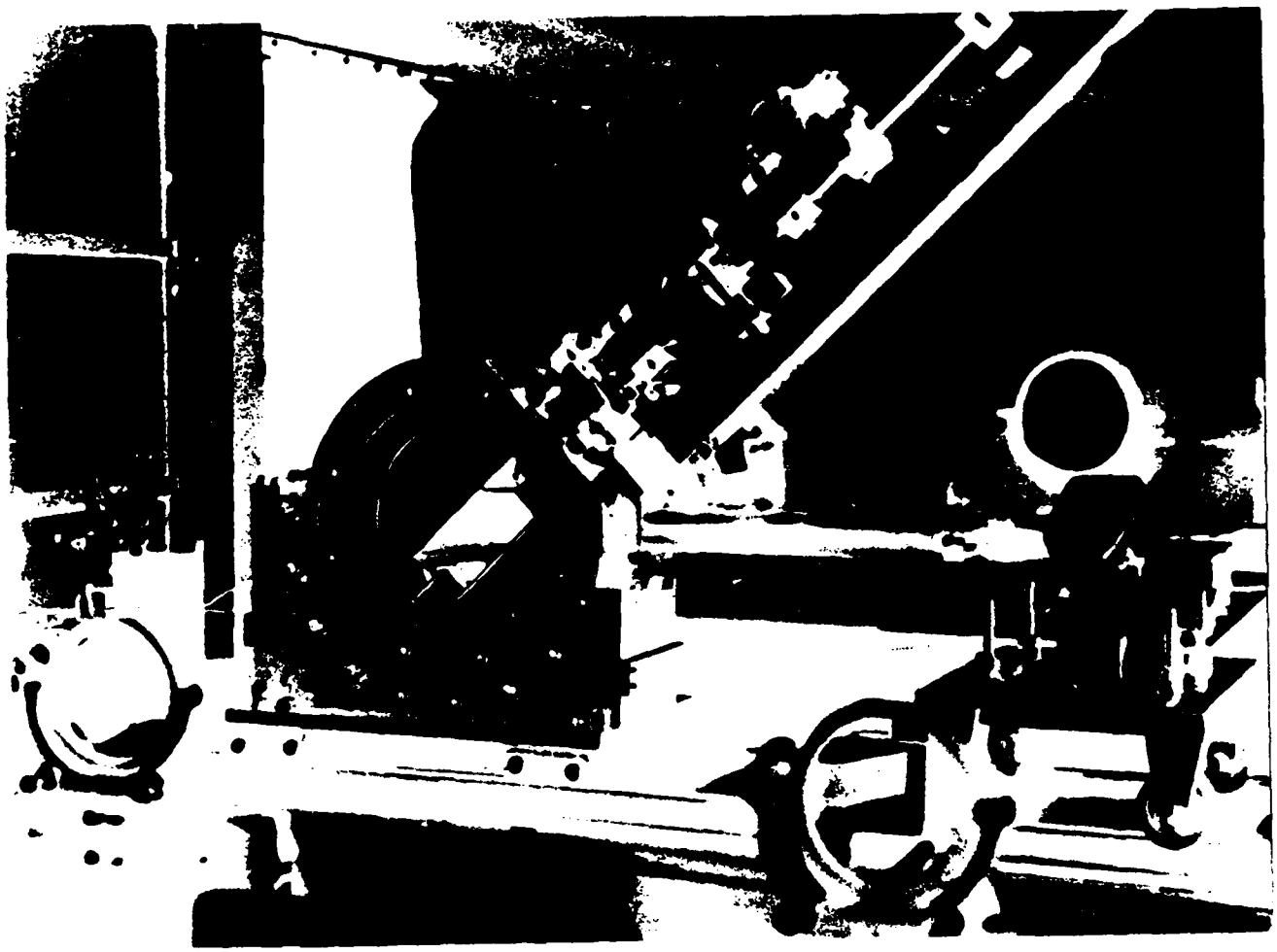

Figure 2

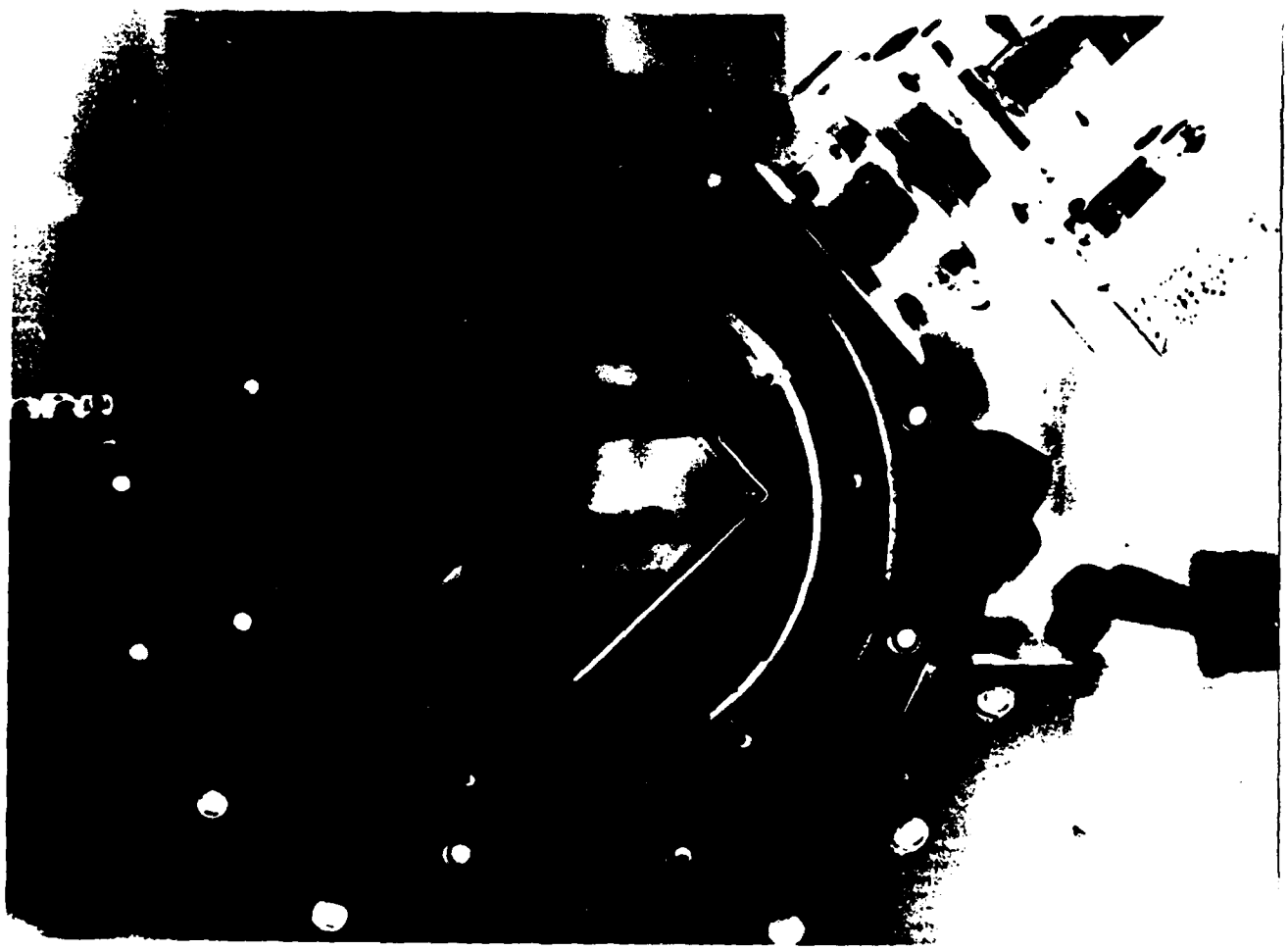

Figure 3

(a)

(b)

Figure 4 a & b

(c)

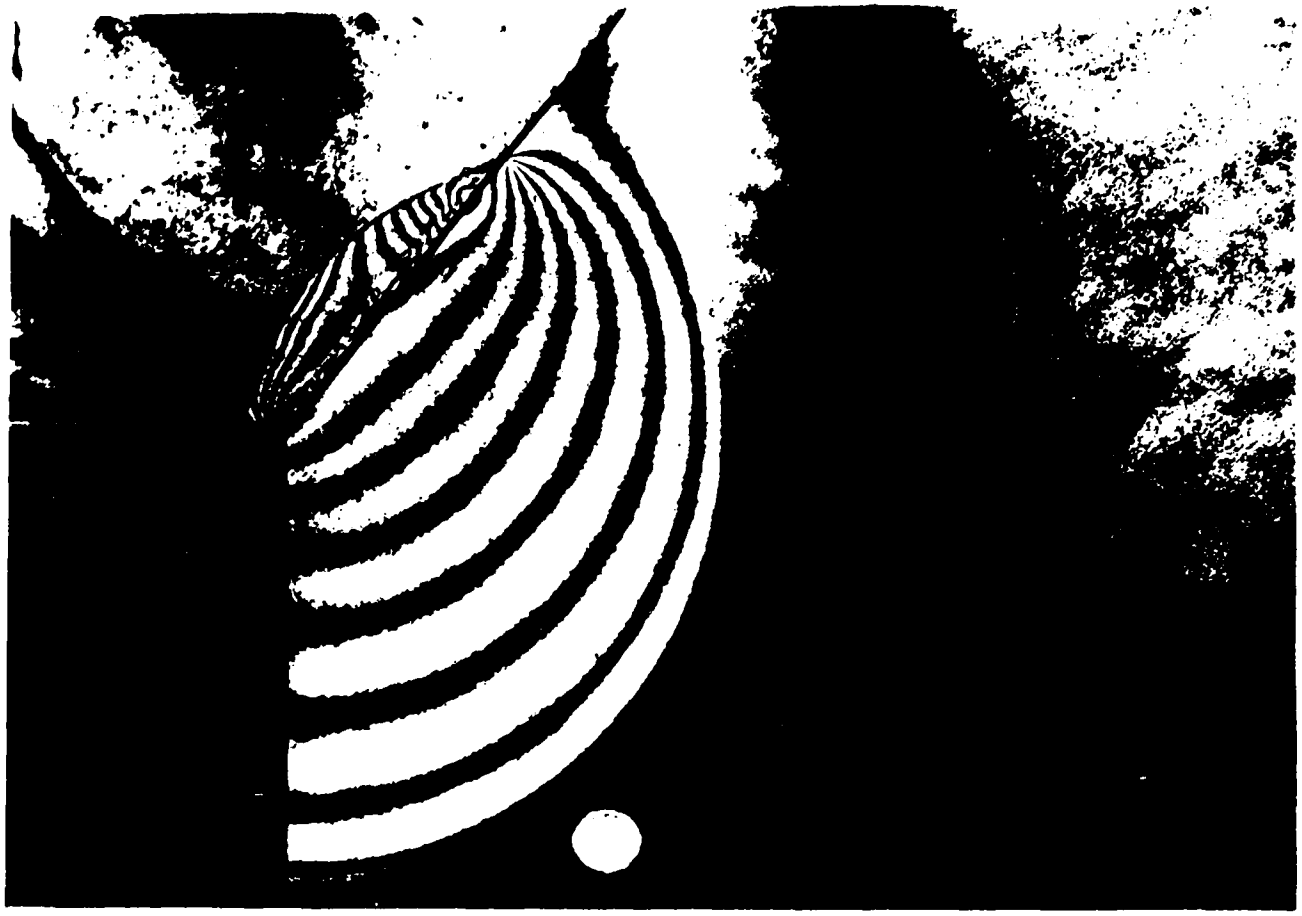

(a)

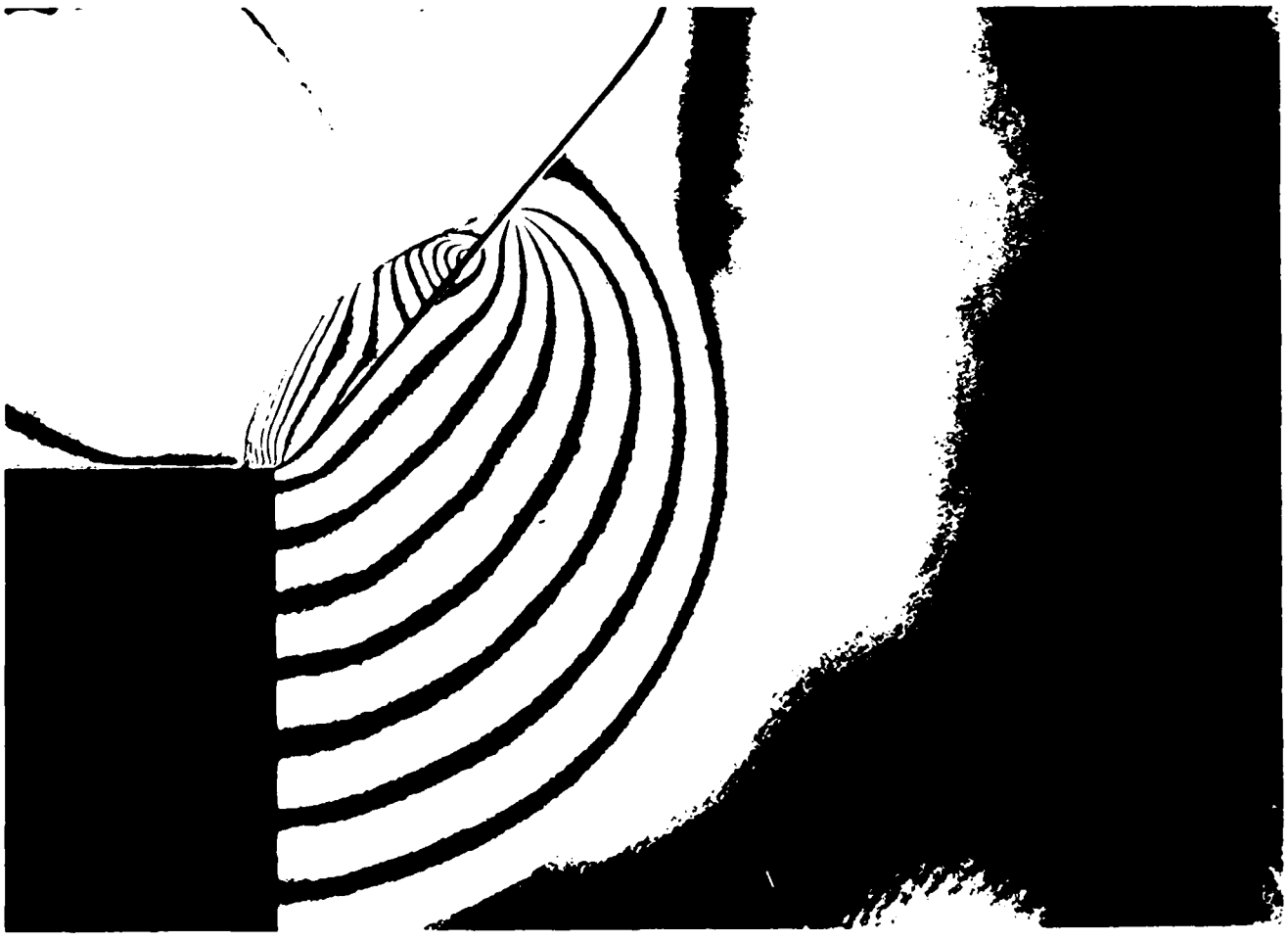

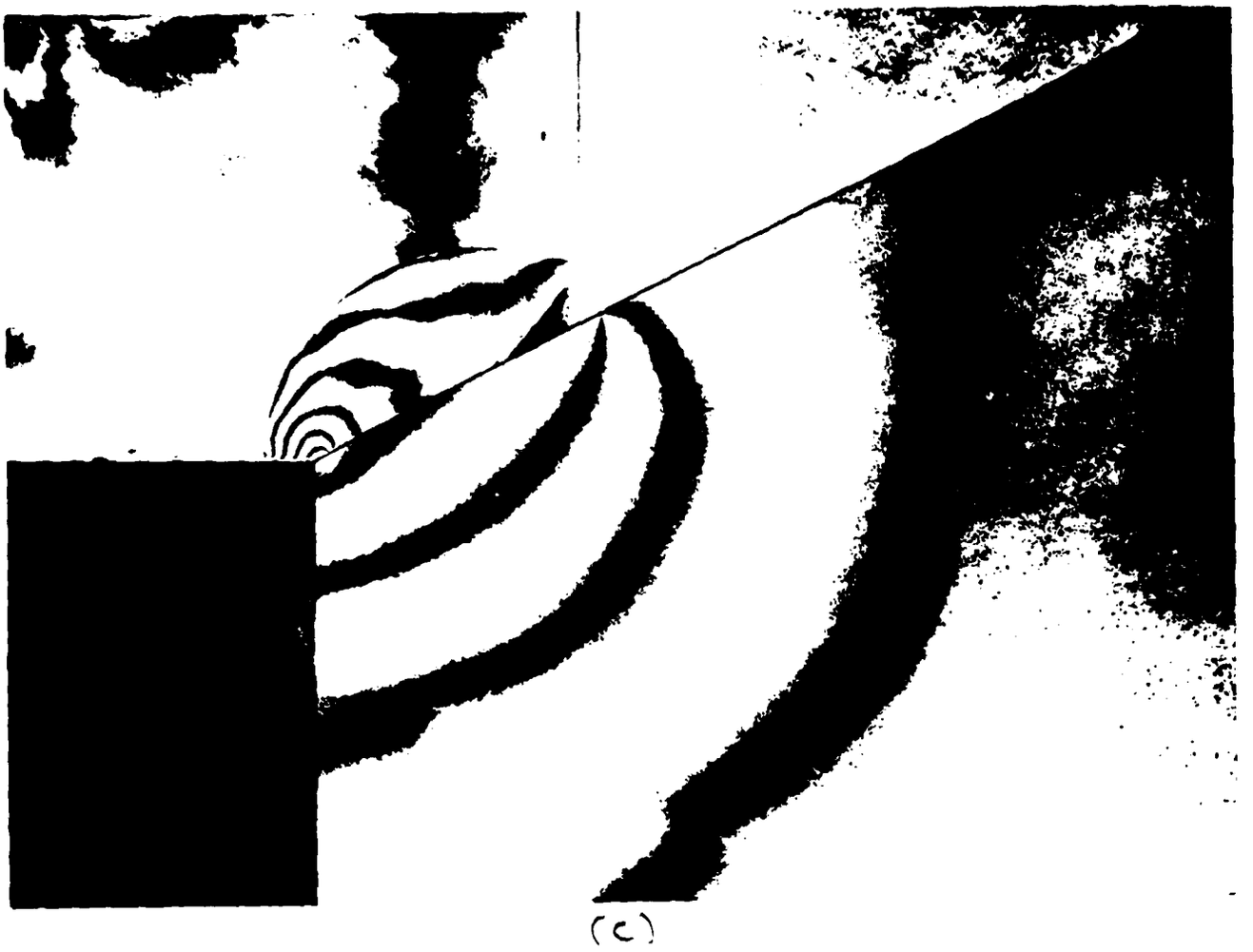

(c)

Figure 5(c)

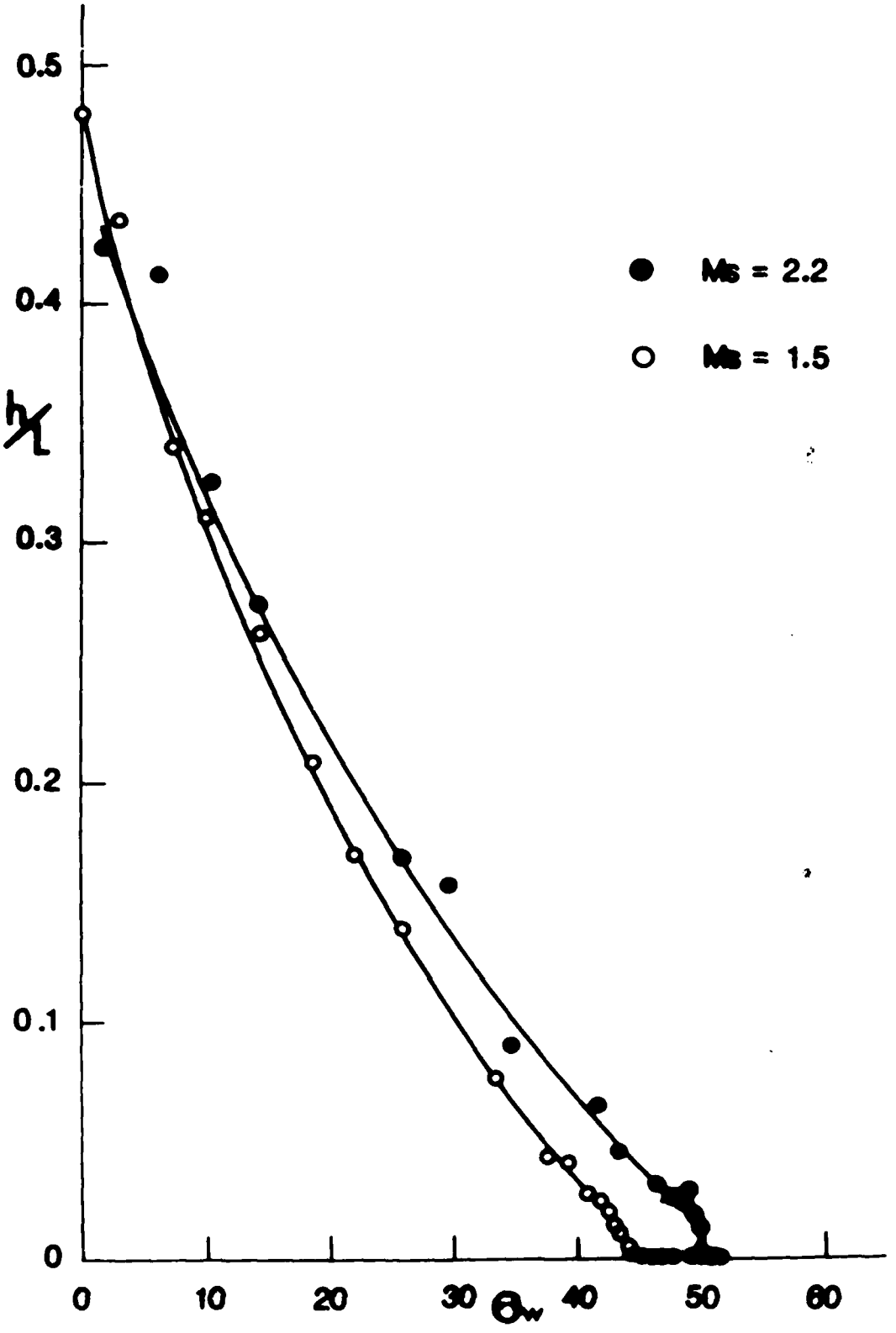

Figure 6

END

FILMED

12-85

DTIC